nature chemical biology

A parallel glycolysis provides a selective advantage through rapid growth acceleration

Richard C. Law [1], Glenn Nurwono [2] & Junyoung O. Park [1] ✉

Glycolysis is a universal metabolic process that breaks down glucose to produce adenosine triphosphate (ATP) and biomass precursors. The Entner–Doudoroff (ED) pathway is a glycolytic pathway that parallels textbook glycolysis but yields half as much ATP. Accordingly, in organisms that possess both glycolytic pathways (for example, *Escherichia coli*), its *raison d'être* remains a mystery. In this study, we found that the ED pathway provides a selective advantage during growth acceleration. Upon carbon and nitrogen upshifts, *E. coli* accelerates growth faster with than without the ED pathway. Concurrent isotope tracing reveals that the ED pathway flux increases faster than that of textbook glycolysis. We attribute the fast response time of the ED pathway to its strong thermodynamic driving force and streamlining of glucose import. Intermittent nutrient supply manifests the evolutionary advantage of the parallel glycolysis; thus, the dynamic nature of an ostensibly redundant pathway's role in promoting rapid adaptation constitutes a metabolic design principle.

By survival of the fittest, modern organisms efficiently use available nutrients and rapidly adapt growth to changing environments[1]. Organisms across the domains of life use glycolysis, or the Embden–Meyerhof-Parnas (EMP) pathway, for efficient generation of energy and biomass precursors[2,3]. Glycolysis responds to environmental perturbations and changing cellular demands by rapidly modulating its flux while maintaining metabolic homeostasis[4].

Most organisms possess alternative glycolytic routes, such as the phosphoketolase pathway[5], the pentose phosphate pathway (PPP) and, common to microorganisms and plants, the Entner–Doudoroff (ED) pathway[6] (Fig. 1a). The EMP textbook glycolysis and the ED glycolysis are parallel from a carbon-centric perspective as both pathways convert one glucose into two pyruvate molecules. The difference is that, compared to textbook glycolysis, which yields two adenosine triphosphate (ATP) and two reduced nicotinamide adenine dinucleotide (NADH) molecules, the ED pathway yields one ATP, one NADH and one reduced nicotinamide adenine dinucleotide phosphate (NADPH) (Fig. 1b). Despite the less efficient ATP generation, some microorganisms

exclusively use the ED pathway due to its lower protein burden (that is, fewer reaction steps) and higher exergonicity (that is, greater thermodynamic driving force) (Fig. 1b) compared to textbook glycolysis[7–9].

Interestingly, many organisms, including 14% of genome-annotated prokaryotes, possess both the EMP and ED pathways[7]. Despite the apparent redundancy, the ED pathway facilitates sugar acid (including gluconate) catabolism[10] and genetic resilience[11–13]. The two glycolytic pathways also have different transcriptional regulation mechanisms[14]. In *E. coli*, the unique intermediate of the ED pathway 2-keto-3-deoxy-6-phosphogluconate (KDPG) deactivates transcriptional repressor YebK, which is implicated in determining the duration of the lag phase during nutrient downshift[15]. However, understanding of the ED pathway is still limited compared to that of the EMP pathway[16]. Furthermore, there is no clear experimental support for an evolutionary advantage of concurrent utilization of the parallel glycolytic pathways.

We were curious why an organism would retain and operate the ED pathway when it already has the EMP pathway that generates ATP more efficiently. We sought to identify conditions in which the ED

[1]Department of Chemical and Biomolecular Engineering, University of California, Los Angeles, Los Angeles, CA, USA. [2]Department of Chemistry and Biochemistry, University of California, Los Angeles, Los Angeles, CA, USA. ✉e-mail: jop@ucla.edu
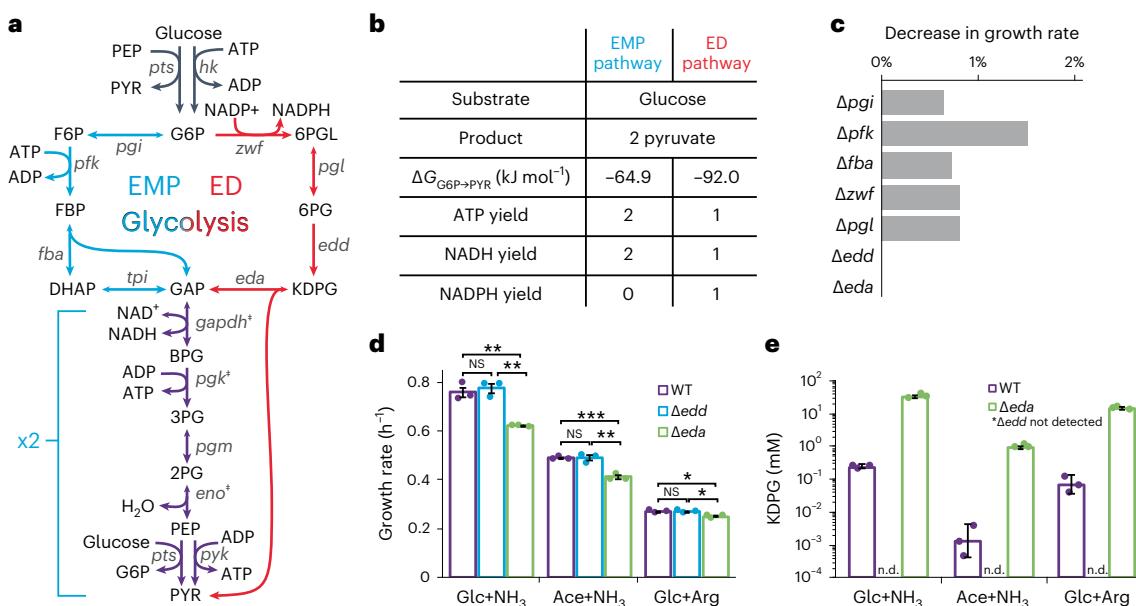
Fig. 1 | The ED pathway is a parallel glycolytic pathway that does not affect cell growth rate. a, EMP glycolysis (red) and ED glycolysis (blue) are parallel, and they share the steps of lower glycolysis (purple). Essential genes are marked with ‡. **b**, The EMP and ED pathways are parallel carbon-wise with a bioenergetic difference. The ED pathway is thermodynamically more forward-driven (that is, ΔG is more negative). **c**, The impact of single non-essential gene knockouts on growth rate was predicted with FBA. **d**, WT and ED-pathway-deficient (that is, Δedd and Δeda) strains were grown in minimal media with glucose or acetate as the sole carbon source and ammonia or arginine as the sole nitrogen source. Their exponential growth rates were measured. *$P < 0.05$, **$P < 0.01$ and ***$P < 0.001$ by a two-tailed t-test. P values from left to right, top to bottom, are as follows: 0.003, 0.0014, 0.0009, 0.003, 0.015 and 0.012. **e**, The absolute concentrations of the ED pathway intermediate KDPG were measured in WT, Δedd and Δeda strains on the different carbon and nitrogen sources using LC–MS and an authenticated standard. Error bars represent the s.e.m. with $n = 3$ biological replicates. 2PG, 2-phosphoglycerate; 3PG, 3-phosphoglycerate; 6PGL, 6-phosphogluconolactone; 6PG, 6-phosphogluconate; BPG, 1,3-bisphosphoglycerate; DHAP, dihydroxyacetone phosphate; F6P, fructose-6-phosphate; FBP, fructose-1,6-bisphosphate; G6P, glucose-6-phosphate; GAP, glyceraldehyde-3-phosphate; NS, not significant; PEP, phosphoenolpyruvate; PYR, pyruvate. pts represents the gene(s) for phosphotransferase system; hk, hexokinase; pgi, phosphoglucoisomerase; pfk, phosphofructokinase; fba, fructose bisphosphate aldolase; tpi triose phosphate isomerase; zwf, glucose-6-phosphate dehydrogenase; pgl, 6-phosphogluconolactonase; edd, phosphogluconate dehydratase; eda, 2-dehydro-3-deoxy-phosphogluconate aldolase; $gapdh$, glyceraldehyde-3-phosphate dehydrogenase; pgk, phosphoglycerate kinase; pgm, phosphoglycerate mutase; eno, enolase; pyk, pyruvate kinase.

pathway's contribution to cells becomes meaningful. In stable nutrient environments, knocking out the ED pathway in *E. coli* had a negligible effect on cell growth. When we subjected the cells to nutrient upshift, however, the initial acceleration of growth of the ED-pathway-capable strain was substantially faster than that of the knockout strain. We found this difference to occur on a fast timescale (<10 minutes) during which cells would exhibit a metabolic response without substantial proteome reallocation.

To gain a mechanistic insight into the observed growth dynamics, we developed a strategy for discerning the fluxes through the two glycolytic pathways. Using stable isotope tracers and liquid chromatography–mass spectrometry (LC–MS), we observed that the ratio of ED to EMP pathway fluxes rapidly increased to 20% upon nitrogen upshift and 130% upon carbon upshift. Thus, the ED pathway aided cells in meeting the rapidly increasing energetic and carbon demand. This transitory metabolic benefit underlay the selective advantage of parallel glycolysis under intermittent nutrient availability. We surmise that organisms may employ parallel pathways elsewhere in metabolism to promote rapid adaptation in dynamic environments.

Results

The ED pathway does not affect growth rates

To assess the contribution of the EMP and ED glycolytic enzymes on growth rates, we performed flux balance analysis (FBA) on the genome-scale metabolic model of *E. coli* (iAF1260)[17]. We simulated knocking out individual non-essential genes of the EMP and ED glycolysis and determined the maximum growth rates within the feasible flux space (Fig. 1c). Unlike the EMP pathway genes, which slowed growth upon knockout, the ED pathway genes had no effect on growth rates. We validated FBA predictions experimentally by comparing the growth rates of *E. coli* with and without the ED pathway genes (that is, wild-type (WT) versus Δedd versus Δeda) under various nutrient conditions (Fig. 1d). The WT and Δedd strains had indistinguishable growth rates, corroborating our FBA simulations. We observed a 17% slowdown of growth in the Δeda strain. This difference was attributable to a 100-fold buildup of the ED pathway intermediate KDPG to as much as 34 mM in the Δeda mutant (Fig. 1e), whose accumulation is correlated with bacteriostasis[18]. Nonetheless, clean elimination of the ED pathway in the Δedd strain showed that the ED pathway itself exerted a negligible direct effect on exponential growth rates.

Parallel glycolysis promotes rapid growth acceleration

A key trait of modern organisms is their ability to quickly detect and use scarce nutrient resources once they become available[19,20]. Because WT and Δedd strains showed no differences in stable environments, we investigated the role of the ED pathway during dynamic adaptation. We subjected these two strains to carbon or nitrogen upshift, a transition from a nutrient-limited to a replete state. Carbon limitation was achieved by using minimal media with a less favorable carbon source acetate in lieu of glucose. Acetate forces cells to use the glyoxylate shunt and gluconeogenesis to produce larger carbon backbones and supports slow growth[21,22]. Nitrogen limitation was introduced by culturing cells in a low initial NH_4Cl concentration (2 mM), which gets depleted and stalls cell growth, or replacing NH_4Cl with arginine, a less favorable nitrogen source[23]. We induced upshift by spiking in glucose and NH_4Cl to carbon-limited and nitrogen-limited cultures, respectively.
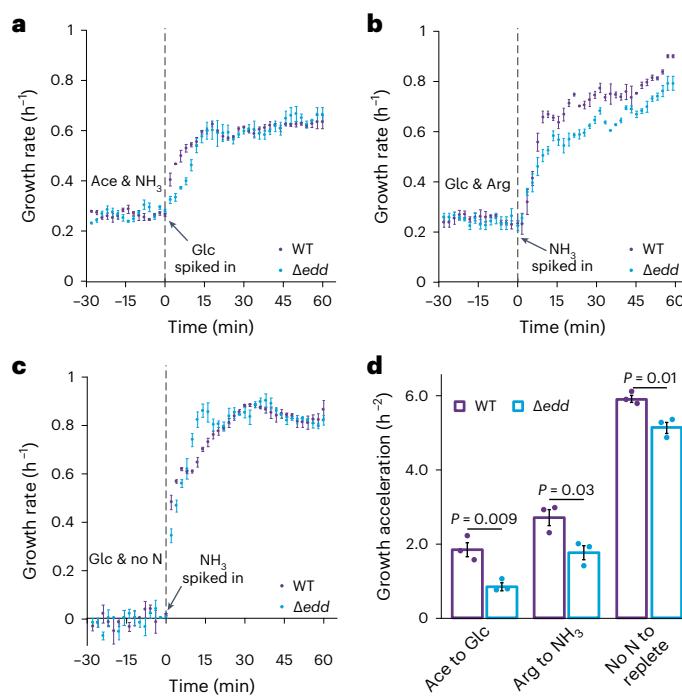
Fig. 2 | ED glycolysis promotes rapid growth acceleration upon nutrient upshift. a, WT and Δ*edd* strains had been grown in minimal media with acetate as the sole carbon source, and at $t = 0$ min glucose was spiked in at 0.2% (w/v). Growth rates were measured continuously during the carbon upshift. **b**, Similarly, growth rates of WT and Δ*edd* cells in glucose minimal media were measured during nitrogen upshift from arginine as the sole nitrogen source to 10 mM NH₄Cl. **c**, WT and Δ*edd* strains had been grown in limited ammonia media until nitrogen was depleted and growth stagnated, and at $t = 0$ min NH₄Cl was spiked in at 10 mM. **d**, The maximum acceleration of growth was quantified by taking the time derivative of growth rates in the first 6–10 min of each nutrient upshift. Error bars represent the s.e.m. ($n = 3$ biological replicates). P values were obtained by two-tailed t-tests.

Upon upshift, both WT and Δ*edd* strains immediately increased growth rates (Fig. 2). However, the transition paths from slow to fast growth differed between the two strains. Upon carbon upshift, WT cells increased growth faster than Δ*edd* cells and maintained faster growth for 15 minutes until they both reached stable growth (Fig. 2a and Extended Data Fig. 1a). This trend was similar in the arginine-to-NH₄Cl nitrogen upshift, in which WT cells accelerated growth and maintained faster growth than Δ*edd* cells for 1 hour until the two strains reached the same stable growth rate (Fig. 2b and Extended Data Fig. 1b). For NH₄Cl depletion to repletion, WT displayed a higher initial acceleration of growth in the first 6 minutes, but the Δ*edd* strain outpaced WT in the subsequent 10 minutes (Fig. 2c). Although the nitrogen upshifts brought both strains to the stable growth rate of ~0.8 h⁻¹ as in the nutrient-replete state, the carbon upshift did not. The incomplete recovery of the growth rate was due to the presence of high external acetate, which depletes intracellular metabolic intermediates that contribute to biomass synthesis[24] (Extended Data Fig. 1c). These observations suggested that the ED pathway contributes to the faster growth acceleration during nutrient upshift.

To quantify this difference in growth dynamics, we computed growth acceleration, which is the time derivative of the specific growth rate (μ), which is the time derivative of log culture density. The maximal growth acceleration occurred in the first few (6–10) minutes of all upshifts, and WT consistently outpaced Δ*edd* during this period (Fig. 2d). Carbon upshifts from glycerol and succinate, which are lower glycolytic and tricarboxylic acid (TCA) cycle intermediates, to glucose

showed similar trends of higher maximum acceleration in WT cells than in Δ*edd* cells (Extended Data Fig. 2a). Unlike other upshifts, carbon upshift from mannose to glucose resulted in a muted initial (first 8 minutes) growth acceleration in both WT and Δ*edd* cells, followed by Δ*edd* cells accelerating growth faster than WT cells in the subsequent 8 minutes (Extended Data Fig. 2b). The delayed and reversed growth acceleration hinted at a bottleneck in glucose uptake during upshift due to competition between glucose and mannose for the phosphotransferase system (PTS)[25]. When carbon upshift obviated the need for glycolysis (for example, acetate to succinate), growth acceleration was similar between the two strains (Extended Data Fig. 2c). This rapid growth acceleration (except for the case of upshift from one PTS sugar to another) reflected metabolic rewiring that is driven by changes in metabolite levels rather than enzyme levels.

Both glycolytic pathways activate upon nutrient upshift

We sought to gain mechanistic insights into the disparate growth acceleration with and without the ED pathway during nutrient upshift. Using LC–MS, we measured the levels of glycolytic intermediates and co-factors before and shortly after upshift (Fig. 3a). All three nutrient upshifts resulted in rapid changes in metabolite levels, with the carbon upshift inducing the greatest overall change.

In both WT and Δ*edd*, carbon upshift increased the upper EMP glycolytic intermediates and 6-phosphogluconate (6PG) while lowering phosphoenolpyruvate (PEP), which had accumulated in the absence of glucose (Fig. 3a). The decrease in PEP levels reflected the unblocking of the PTS, which phosphorylates glucose using PEP while transporting glucose into the cell, upon glucose addition[26]. In the WT strain, Gibbs free energy change (ΔG) across the EMP and the ED glycolysis became more forward-driven (that is, $\Delta\Delta G < 0$) to −54.8 kJ mol⁻¹ and −87.9 kJ mol⁻¹, respectively, whereas ΔG of gluconeogenesis increased to 8.6 kJ mol⁻¹ ($\Delta\Delta G = +10.8$ kJ mol⁻¹) in 3 minutes of carbon upshift (Fig. 3b and Supplementary Note 1). Thus, the rapid metabolic shifts rendered glycolysis thermodynamically more favorable and gluconeogenesis unfavorable in WT. On the other hand, thermodynamic shifts in Δ*edd* were less pronounced (Fig. 3c).

Nitrogen upshift increases glycolytic flux through a combination of upregulation of glucose transport by decreasing α-ketoglutarate (αKG), which inhibits Enzyme I (EI) of the PTS, and decreasing the reversibility of glycolytic steps[27]. Upon nitrogen upshift, the intermediates of glycolysis changed to a smaller extent in WT compared to carbon upshift (Fig. 3a), and, as a result, we observed smaller $\Delta\Delta G$ in both the EMP and the ED glycolysis (Fig. 3b). $\Delta\Delta G$ of glycolytic pathways for Δ*edd* in nitrogen upshift was larger than carbon upshift but otherwise similar to nitrogen upshift in WT (Fig. 3c). Although the initial values of overall ΔG of the EMP and ED pathways were substantially different, their ΔG changed similarly upon carbon and nitrogen upshift due to the similarity in the initial substrates and final products of the parallel pathways. However, the intermediate metabolites unique to each pathway (for example, fructose-1,6-bisphosphate and KDPG), which do not contribute to overall pathway thermodynamics, displayed disparate dynamics (Fig. 3a), suggesting different mechanisms at play in modulating the two glycolytic pathways.

Asymmetric ¹³C-glucose reveals glycolytic fluxes

To quantify fluxes through the parallel glycolytic pathways, we needed a glucose tracer that differentially labels lower glycolytic metabolites depending on the pathway taken. Unlike the EMP glycolysis, in which each glucose produces a pair of triose phosphates (glyceraldehyde-3-phosphate (GAP)) by cleaving fructose bisphosphate down the middle, the ED glycolysis shunts only the fourth, fifth and sixth carbons of glucose to the shared lower glycolysis as a triose phosphate (Fig. 4a). With [1,2-¹³C₂]-glucose, the EMP pathway generates unlabeled (M+0) and doubly labeled (M+2) triose phosphate at a one-to-one ratio, whereas the ED pathway generates only M+0 triose phosphate.
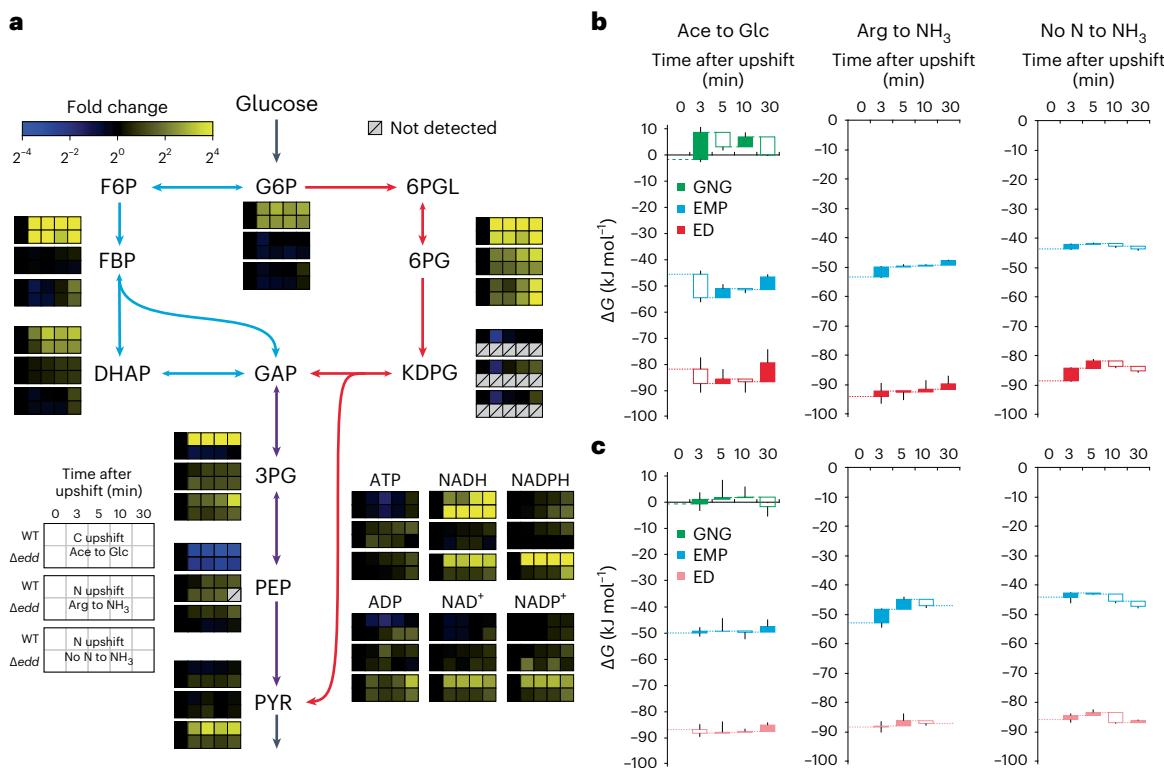
Fig. 3 | Both EMP and ED glycolytic pathways are activated upon nutrient upshift. a, The levels of glycolytic intermediates and co-factors were measured in WT and Δ*edd* strains before and after carbon and nitrogen upshifts using LC–MS. Yellow and blue colors represent higher and lower levels relative to the pre-upshift levels of metabolites at *t* = 0 min. **b,c**, Cumulative Gibbs free energies of reactions (Δ*G*) across the EMP pathway, the ED pathway and gluconeogenesis (GNG) were obtained using the overall net reactions of the pathways and the

concentrations of their initial substrates and final products (Supplementary Note 1) during upshift in WT (**b**) and Δ*edd* (**c**). Because the ED pathway was inactive in Δ*edd*, its Δ*G* is shown in light red. The dotted lines represent the Δ*G* at the previous timepoints. Filled boxes indicate an increase in Δ*G* from the previous state, and empty boxes indicate a decrease. Whiskers represent the s.e.m. (*n* = 3–6 biological replicates).

The EMP and ED glycolysis also result in unique positional isotope labeling of pyruvate (Fig. 4a) that can be distinguished by MS/MS fragmentation of valine (Fig. 4b). Furthermore, tracing [1,2-^{13}C$_2$]-glucose informs us of the oxidative pentose phosphate pathway (OxPPP) flux, which uniquely generates singly labeled (M+1) triose phosphate (Extended Data Fig. 3a). In *E. coli*, exponentially growing in a minimal medium replete with glucose and NH$_4$Cl, 3-phosphoglycerate (3PG) and valine labeling measurement indicated a slow ED pathway flux relative to the EMP glycolysis (Fig. 4a,b).

The non-oxidative pentose phosphate pathway (non-OxPPP) and the reversibility of phosphoglucoisomerase (PGI) potentially obscure our flux quantitation by opening the door for carbons to recursively go through the PPP and produce various isotopomers of triose phosphate[28,29]. To disambiguate the central carbon metabolism fluxes, we also traced [5,6-^{13}C$_2$]-glucose (Fig. 4c). Similar to [1,2-^{13}C$_2$]-glucose, [5,6-^{13}C$_2$]-glucose indicates the relative glycolytic fluxes based on the skewed labeling ratios but with the ED pathway flux contributing to M+2 triose phosphate (Extended Data Fig. 3b). Nonetheless, [5,6-^{13}C$_2$]-glucose had two unique advantages: (1) it revealed that the extent of the PPP recycling, which generates unlabeled 6PG, was small (Fig. 4c); and (2) it solved central carbon metabolism fluxes by a simple orthogonal mass balance, which is attributed to these ^{13}C not being shuffled in the PPP (Extended Data Fig. 3c). Using [1,2-^{13}C$_2$]-glucose and [5,6-^{13}C$_2$]-glucose, we measured the labeling of 3PG, 6PG and valine and solved the fluxes through the EMP pathway, the ED pathway and the PPP (Supplementary Notes 2–4). These approaches revealed the ED pathway flux to be small compared to the EMP pathway flux (ED-to-EMP flux ratio was between 0.06 and 0.12) under the nutrient-replete condition.

ED glycolysis accelerates faster than EMP glycolysis

We hypothesized that the adaptive growth advantage of the WT over Δ*edd* was due to the ED pathway enabling higher glycolytic flux in transitional periods. The total glycolytic flux increases during the carbon and nitrogen upshifts. In carbon-limited conditions (that is, acetate but no glucose), glycolytic flux is zero because there is no carbon source available for glycolysis. Thus, carbon upshift to glucose necessarily accelerates glycolytic fluxes. On arginine, the glucose uptake rate of WT cells is 7.29 mmol gCDW^{-1} h^{-1}, and, upon nitrogen upshift, it increases to 11.7 mmol gCDW^{-1} h^{-1} (ref. 27). However, how each glycolytic pathway contributes to the flux acceleration is unknown. Using [1,2-^{13}C$_2$]-glucose and [5,6-^{13}C$_2$]-glucose, we investigated how the use of the parallel glycolytic pathways changed during carbon and nitrogen upshift. Glycolytic intermediates reach a stable labeling within 1 minute (Extended Data Fig. 4a) due to their fast turnover (~1 s^{-1}) (Extended Data Fig. 4b). Thus, their isotopic labeling can be approximated as a series of minute-scale pseudo-steady states. We measured the isotope labeling of 3PG and 6PG from [1,2-^{13}C$_2$]-glucose and [5,6-^{13}C$_2$]-glucose tracers before and 3, 5, 10 and 30 minutes after upshift (Fig. 5a,b and Extended Data Fig. 5a,b).

The ED pathway's contribution to overall glycolysis rapidly increased upon carbon and nitrogen upshifts. Upon carbon upshift, the ED pathway carried the major glycolytic flux, and, after 10 min, the ED-to-EMP flux ratio returned to the stable value observed in the nutrient-replete condition (Fig. 5a). Although we could not quantify the ED pathway flux at 0 minutes (that is, in the carbon-limited condition) due to the absence of ^{13}C glucose tracers, we found that, even on acetate, *E. coli* expressed the ED pathway enzymes (Extended Data Fig. 5c). Because any unlabeled glycolytic intermediates that
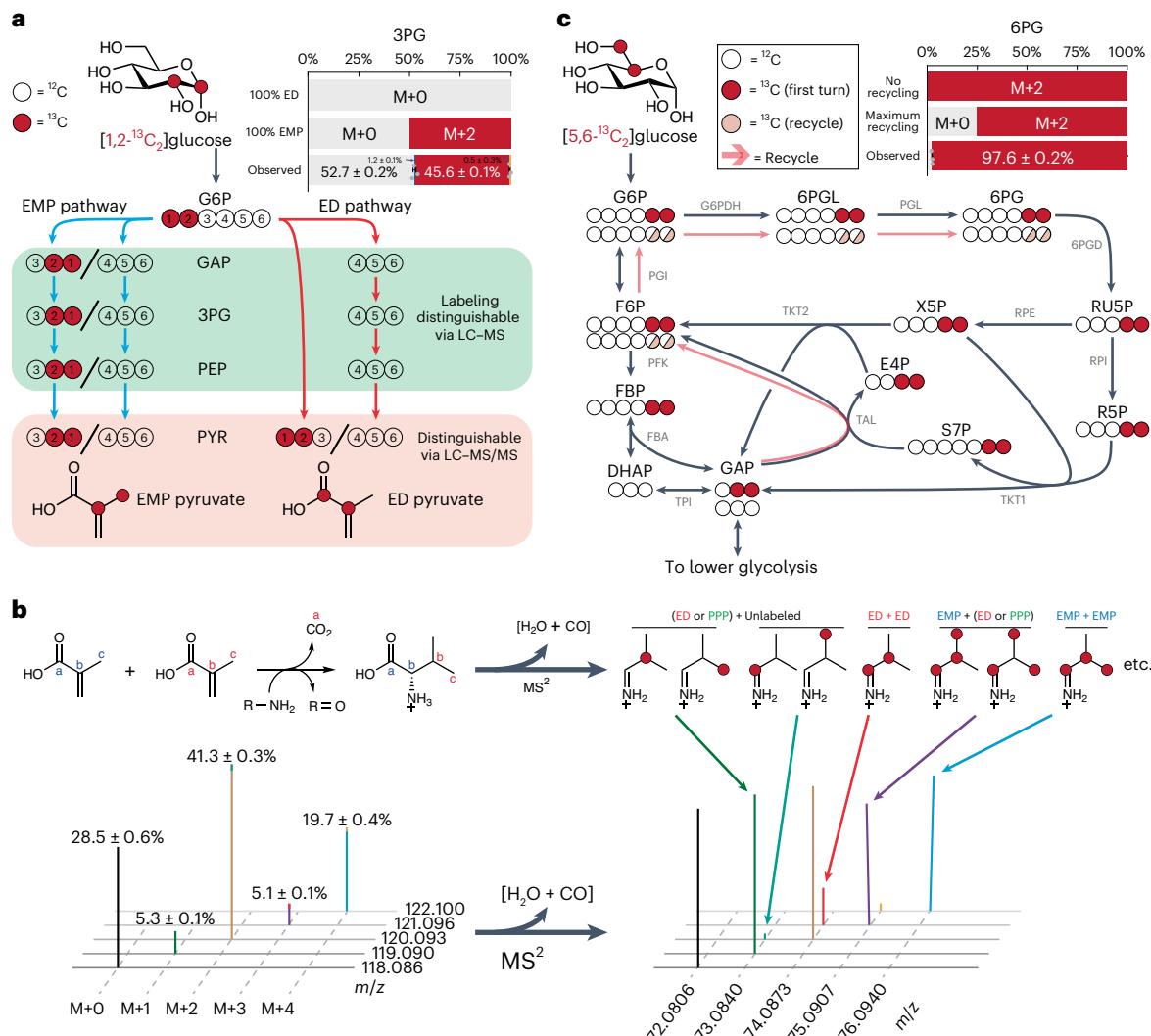
Fig. 4 | Asymmetrically ¹³C-labeled glucose tracers reveal parallel glycolytic fluxes. a, With [1,2-¹³C₂]-glucose, only the EMP glycolysis generates labeled lower glycolytic intermediates. Both the EMP and the ED pathways produced labeled pyruvate but at different positions. The labeling fractions of 3PG in cells without nutrient limitation were measured using LC–MS and used to calculate the ED pathway activity (Supplementary Notes 2 and 3). **b**, Positional labeling of pyruvate was distinguished using LC–MS/MS. Isotopologues of valine, which is synthesized from two pyruvate molecules, were fragmented. The MS² spectra revealed the positional labeling indicative of the ED pathway activity (Supplementary Note 3). **c**, The unlabeled fraction of 6PG from [5,6-¹³C₂]-glucose tracing indicates recursive PPP usage. Unlabeled 6PG is generated only from S7P and unlabeled GAP through the reactions in light red arrows. The labeling fractions of 6PG were measured using LC–MS and used to refine the quantification of glycolytic fluxes. Error bars represent the s.e.m. (*n* = 3 biological replicates). 6PGD, 6-phoshogluconate dehydrogenase; E4P, erythrose-4-phosphate; FBA, fructose-1,6-bisphosphate aldolase; G6PDH, glucose-6-phosphate dehydrogenase; PFK, phosphofructokinase; PGI, phosphoglucoisomerase; PGL, phosphogluconolactonase; R5P, ribose-5-phosphate; RPE, ribulose phosphate epimerase; RPI, ribose phosphate isomerase; RU5P, ribulose-5-phosphate; S7P, sedoheptulose-7-phosphate; TAL, transaldolase; TKT1 and TKT2, transketolase; TPI, triose phosphate isomerase; X5P, xylulose-5-phosphate.

had been derived from unlabeled acetate affect our ability to compute glycolytic fluxes accurately, we took extra caution by performing acetate-to-[U-¹³C₆]-glucose upshift to account for residual acetate-derived intermediates (Extended Data Fig. 5d and Supplementary Note 4). Both nitrogen upshifts from arginine and low NH₄Cl rapidly increased the relative ED pathway flux (Fig. 5b). The extent of the ED pathway utilization during nitrogen upshift was smaller than that of carbon upshift, testifying to the need for a reliable glycolytic route even in thermodynamically less favorable times of early carbon upshift.

Contemporaneous with the increasing relative importance of the ED pathway, the absolute glucose uptake rates (that is, total glycolytic fluxes) shot up upon nutrient upshifts (Fig. 5c). Within 5 minutes of glucose and NH₄Cl addition to carbon-limited and nitrogen-limited cells, respectively, glucose uptake rates increased by as much as

40 mmol gCDW⁻¹ h⁻¹ and as little as 2 mmol gCDW⁻¹ h⁻¹, with WT cells displaying greater acceleration than Δ*edd* cells. Taken together, our flux quantitation revealed that, whereas the EMP pathway is the main stable glycolytic route, the ED pathway responds faster to upshift glycolysis (Fig. 5d). This faster acceleration of the ED pathway flux was consistent with our earlier observation that the ED pathway-capable WT accelerated growth faster than the Δ*edd* ED pathway knockout strain, even though they grew equally well under stable nutrient conditions.

Intermittent feeding favors parallel glycolysis

What is the evolutionary benefit of the parallel ED glycolysis? In nature, access to favorable nutrients is often limited because their supply is intermittent and subject to competition within microecosystems[30]. To answer this question, we cultured WT and Δ*edd* strains on low

Fig. 5 | The ED pathway flux accelerates faster than the EMP glycolytic flux.
a, The ED-to-EMP flux ratios were obtained using the 3PG labeling from [1,2-^{13}C$_2$]-glucose (green) upon carbon upshift. Due to some residual gluconeogenic activity, the 3PG labeling fractions were corrected using the mirror-image tracer [5,6-^{13}C$_2$]-glucose (blue) (Supplementary Note 4). **b**, The ED-to-EMP flux ratios were measured during nitrogen upshift from arginine (red) and no nitrogen (yellow). **c**, Instantaneous glucose uptake rates (that is, total glycolytic fluxes) were measured by the extent of accumulation of a G6P analogue 2-deoxyglucose-

6-phosphate in WT and Δ*edd* cells that were incubated with 2-deoxyglucose for 5 s at different timepoints of nutrient upshift. Statistical significance between the two strains was obtained by two-way ANOVA using strain and time as two variables. **d**, The EMP and ED pathways have complementary roles. The EMP pathway maintains high homeostatic glycolytic flux, and the ED pathway rapidly bolsters glycolytic flux upon increased biomass and energy demand. Error bars represent the s.e.m. (*n* = 3 biological replicates).

glucose or low ammonia until the limiting nutrient was depleted and spiked in a low dose of the nutrient repeatedly after nutrient depletion. Under these intermittent nutrient feeding conditions, cells possessing both glycolytic pathways achieved increasingly denser cultures than Δ*edd* cells (Fig. 6a). In three cycles of glucose upshift, WT achieved a cell density that is 15% higher than that of Δ*edd*. Similarly, four cycles of ammonia upshift widened the growth gap between the two strains to 5%. To test the competitiveness of the cells with parallel glycolysis in the community context, we repeated the intermittent feeding experiments with co-cultures of WT and Δ*edd* cells that expressed a green and a red fluorescent protein, respectively, and counted them using flow cytometry. Regardless of the initial ratio of WT to Δ*edd* cells, the proportion of ED-pathway-capable WT cells became increasingly higher over upshifts (Fig. 6b and Extended Data Fig. 6).

We further investigated the evolutionary relevance of the ED pathway using the *E. coli* long-term evolution experiment (LTEE)[31]. In the LTEE, 12 initial populations derived from REL606 and REL607 strains have been intermittently fed limiting amounts (25 mg L^{-1}) of glucose over 70,000 generations. The low glucose concentration led to glucose depletion, and daily subculturing into fresh media introduced carbon upshift every ~6.6 generations (Fig. 6c).

We analyzed the genome sequences of the 12 populations over 50,000 generations. The accumulation of random and independent mutations would lead to mutation counts in individual genes approximating a Poisson distribution. Instead, we observed more than expected genes with two or more mutations (Extended Data Fig. 7a,b). Some genes even accumulated as many as 50 mutations across the 24 evolved strains (Extended Data Fig. 7c,d). Thus, the mutation history was suggestive of increasing adaptability to intermittent glucose supply.

We compared the mutation history of the EMP and ED glycolytic pathways relative to other pathways. The ED pathway was highly mutated early on, reaching the 96th percentile of pathway mutations by 5,000 generations, whereas the EMP pathway was at the 67th percentile (Fig. 6d and Extended Data Fig. 8a). At 5,000 generations, none of the mutations in these pathways was silent (Extended Data Fig. 8b). In subsequent generations, the percentile ranks of both glycolytic pathways decreased, but the fractions of non-synonymous and indel mutations remained above 50%. With mutations in earlier generations generally leading to a greater increase in the fitness of an organism[32,33], the early mutations in the ED pathway manifested its importance under intermittent glucose supply. We probed the evolutionary interactions between the EMP and ED pathways. Up to 30,000 generations, mutations occurred in either of the two glycolytic pathways (Fig. 6e). Furthermore, by 50,000 generations, 82% of those strains that carried mutations in glycolysis had only one of the two glycolytic pathways mutated (Extended Data Fig. 8c). These observations hint at the distinct utility of the EMP and ED glycolysis in stable and transitional periods.

To experimentally validate the competitiveness of evolved strains in dynamic environments, we subjected the LTEE strains to carbon upshifts and measured their growth acceleration. We selected three of the 12 populations (Ara+3, which had the most mutations in the ED pathway genes; Ara+5, which had the lowest overall mutations; and Ara−2, which had the most mutations outside of the ED pathway genes) at 5,000th and 50,000th generations (Extended Data Fig. 8d). Upon upshift from carbon starvation, acetate, glycerol or mannose to glucose, we found the general tendency of faster growth acceleration in strains evolved over 50,000 generations compared to the ancestral strain (Extended Data Fig. 8e). The strain from Ara+3 displayed
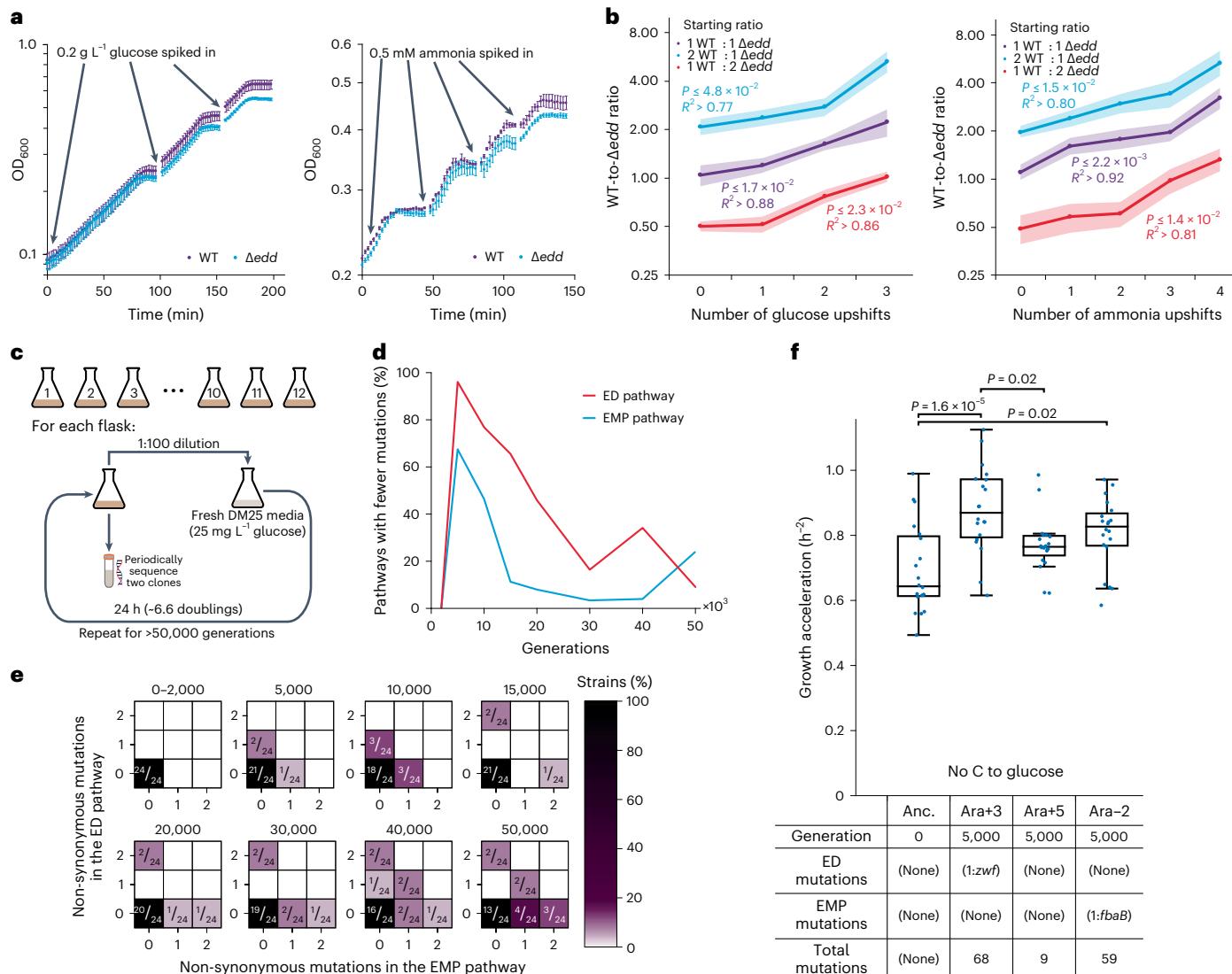
Fig. 6 | The evolutionary benefit of the ED pathway emerges in intermittent nutrient feeding. a, WT and Δ*edd* strains were grown under intermittent supply of glucose or ammonia. Cultures were periodically spiked with low concentrations of glucose or ammonia shortly after growth halted. Error bars represent the s.e.m. (n = 3 biological replicates). **b**, Co-cultures of WT and Δ*edd* strains at varying initial WT-to-Δ*edd* ratios were subjected to intermittent feeding of glucose or nitrogen. WT and Δ*edd* cells, which were tagged with green and red fluorescent proteins, respectively, were counted via flow cytometry. Shaded areas represent the s.e.m. (n = 3 biological replicates). Reported statistics were calculated by linear regression with fixed intercepts for individual biological replicates of the WT-to-Δ*edd* ratio over time. Maximum P values and minimum R^2 values of biological replicates are shown. **c**, In the LTEE, 12 cultures of *E. coli*

were transferred to fresh low-glucose media daily, inducing carbon upshift. From each culture, two clones were periodically sequenced. **d**, Development of non-synonymous mutations and indels in the EMP and ED pathways over 50,000 generations was compared to that of randomly sampled gene groups. **e**, The mutation history of the EMP and ED pathways was monitored in all 24 sequenced strains over 50,000 generations. **f**, The ancestral strain and Ara+3, Ara+5 and Ara−2 strains isolated in the 5,000th generation were subjected to upshift from carbon starvation to glucose, and their growth acceleration was measured. Each box shows the three quartiles, and whiskers extend to the minimum and maximum values within 1.5-fold of the interquartile range (n = 20 biological replicates). Statistical significance between strains was obtained by one-way ANOVA with Tukey's honestly significant difference test for multiple comparison.

the fastest mean growth acceleration during no-carbon-to-glucose and acetate-to-glucose upshifts. Based on these results and power analysis, we obtained sample sizes that would provide sufficient statistical power for testing the growth acceleration of the Ara+3 strain versus the ancestral and other strains at 5,000th generation. Upon glucose addition to acetate-fed and carbon-starved cultures, the Ara+3 and Ara−2 strains accelerated growth, significantly (α = 0.05) faster than the ancestral strain (Extended Data Fig. 8f), with the Ara+3 strain showing the highest improvement in growth acceleration (Fig. 6f). Taken together, short-term and long-term intermittent feeding of glucose pointed to the adaptive and evolutionary importance of parallel glycolysis.

Discussion

Parallel reactions and pathways are prevalent in metabolism, yet the evolutionary advantage of their concurrent utilization remains incompletely understood. In bacteria, the PTS carries out the same function as the glucose transporter, hexokinase and pyruvate kinase[34]. In eukaryotes, parallel pathways are commonly found in different organelles (for example, one-carbon metabolism and partially the TCA cycle in the cytosol and mitochondria)[35–37]. Genetic redundancy is commonplace in diploids[13]. In all organisms, multiple isoforms of various enzymes exist.

The EMP and ED pathways are parallel glycolytic pathways that perform perhaps the most foundational task in metabolism. In an organism with both glycolytic pathways, it is expected that they both

play important roles lest one of them be deprecated. Interestingly, in stable environments, the ED pathway flux in *E. coli* is a small fraction of the EMP glycolysis, and when we knocked out the ED pathway, we did not find any growth defects.

Instead, we found the benefit of the ED pathway to emerge during transitional periods after nutrient upshift. In the first few minutes of carbon and nitrogen upshifts, cells with the ED pathway accelerated growth faster than those without. The quantitation of the EMP and ED glycolytic fluxes revealed the disproportionately fast increase of the ED pathway flux concurrently with the fast growth acceleration. Thus, ED glycolysis is designed to jump once scarce nutrients become available, whereas EMP glycolysis, although slower to respond to nutrient upshift, is designed to efficiently generate ATP under stable environments. The parallel glycolytic pathways are complementary and ensure that organisms are evolutionarily competitive in both stable and dynamic environments.

How does the ED pathway facilitate faster acceleration of growth? At least three factors are at work: thermodynamic driving force, small-molecule-mediated regulation dictating rapid glucose import and NADPH generation. In the carbon upshift experiment, the absence of glucose forces cells to halt glycolysis and use gluconeogenesis. The addition of glucose initiates a switch from gluconeogenesis to glycolysis, which requires flipping the sign of ΔG of every EMP glycolysis reaction step that participates in gluconeogenesis[4,38]. On the other hand, the ED pathway steps do not participate in gluconeogenesis due to highly negative $\Delta G'^\circ$ and, thus, can more readily increase its flux upon glucose addition. The ED pathway also generates NADPH as the OxPPP does but without decarboxylation. Thus, in addition to facilitating rapid glycolytic response and ATP production, another role of the ED pathway is rapid carbon-efficient NADPH production (Extended Data Fig. 9a). By feeding [1-^{2}H]-glucose and [3-^{2}H]-glucose to cells, we observed NADPH labeling through glucose-6-phosphate dehydrogenase (shared between the ED pathway and the OxPPP) that is three times as high as NADPH labeling through the OxPPP-exclusive step 6-phosphogluconate dehydrogenase (Extended Data Fig. 9b). This deuterated glucose tracing experiment revealed that the contributions of the ED pathway and the OxPPP to NADPH production are similar.

The mechanism behind increasing glycolytic flux upon nitrogen upshift differs from that of carbon upshift. In nitrogen limitation, cells voluntarily limit their glucose import via competitive inhibition of the PTS EI by αKG. The PTS is the main glucose transporter that requires PEP as the initial substrate. In glucose limitation, PEP accumulates and acts as a reserve pool ready to increase the PTS flux as soon as glucose becomes available[26]. This is not the case for nitrogen limitation and upshift. Instead, the rapid increase of the ED pathway flux helps cells procure PEP on demand. The ED pathway converts glucose to pyruvate in five reaction steps, and pyruvate can be converted to PEP via phosphoenolpyruvate synthase (PpsA). Along with the PTS, PpsA is regulated by nitrogen availability with αKG acting as its inhibitor that blocks phosphotransfer[39]. Although PpsA reaction sacrifices ATP, which is not a concern for nitrogen-limited cells, the concerted regulation of PpsA and PTS facilitates streamlined glucose transport that supports a rapid increase of carbon supply, energy generation and growth during nitrogen upshift. The ED pathway plays a crucial role in bridging the PTS and PpsA steps via a productive shortcut (Extended Data Fig. 9c).

In nature, rapid nutrient upshift is a common occurrence, and nutrients are gradually depleted by organisms. Bacteria readily adapt to these nutrient fluctuations[40] and have evolved to cope with short-term changes[41]. Our intermittent feeding experiments corroborated the adaptive advantage of the parallel ED glycolysis. Our analysis of the LTEE demonstrated the evolutionary importance of the ED pathway. Had it not played an influential role in repeated glucose upshifts, its mutation history would be unlikely to see such high activities in early generations.

Conventional wisdom has it that parallel pathways afford flexibility. By employing different co-factors and substrate binding affinities

attuned to different environments, parallel reaction steps contribute to metabolic homeostasis under various conditions and stresses[42]. Redundancy could mitigate the negative impacts of one of parallel pathways being misregulated[43]. Enzymes catalyzing the same reactions could also possess different regulatory mechanisms as in the case of self-resistance enzymes that protect cells from natural product inhibitors that they themselves produce[44,45]. Our finding of the dynamic role of the parallel ED glycolysis in promoting rapid adaptation augments the knowledge base for comprehending parallel metabolic pathways.

Glycolysis is often the highest flux-carrying metabolic pathway in heterotrophic organisms. The co-existence of the EMP and ED glycolytic pathways acts as structural support for rapid glycolytic flux control. Such 'hardwired' flux control mechanisms add to the arsenal of rapid adaptation strategies that include small-molecule-based regulation, thermodynamic shift and post-translational modification[46,47]. Alternative glycolytic pathways are not unique to prokaryotes[6,48], and parallel pathways are commonly found in metabolic networks. Thus, we postulate that the *raisons d'être* of parallel metabolic pathways underlie a metabolic design principle in dynamic environments.

Online content

Any methods, additional references, Nature Portfolio reporting summaries, source data, extended data, supplementary information, acknowledgements, peer review information; details of author contributions and competing interests; and statements of data and code availability are available at https://doi.org/10.1038/s41589-023-01395-2.

References

1. Basan, M. et al. A universal trade-off between growth and lag in fluctuating environments. *Nature* **584**, 470–474 (2020).
2. Romano, A. H. & Conway, T. Evolution of carbohydrate metabolic pathways. *Res. Microbiol.* **147**, 448–455 (1996).
3. Bar-Even, A., Flamholz, A., Noor, E. & Milo, R. Rethinking glycolysis: on the biochemical logic of metabolic pathways. *Nat. Chem. Biol.* **8**, 509–517 (2012).
4. Park, J. O. et al. Near-equilibrium glycolysis supports metabolic homeostasis and energy yield. *Nat. Chem. Biol.* **15**, 1001–1008 (2019).
5. Xiong, W. et al. Phosphoketolase pathway contributes to carbon metabolism in cyanobacteria. *Nat. Plants* **2**, 15187 (2015).
6. Chen, X. et al. The Entner–Doudoroff pathway is an overlooked glycolytic route in cyanobacteria and plants. *Proc. Natl Acad. Sci. USA* **113**, 5441–5446 (2016).
7. Flamholz, A., Noor, E., Bar-Even, A., Liebermeister, W. & Milo, R. Glycolytic strategy as a tradeoff between energy yield and protein cost. *Proc. Natl Acad. Sci. USA* **110**, 10039–10044 (2013).
8. Basan, M. et al. Overflow metabolism in *Escherichia coli* results from efficient proteome allocation. *Nature* **528**, 99–104 (2015).
9. Noor, E. et al. The protein cost of metabolic fluxes: prediction from enzymatic rate laws and cost minimization. *PLoS Comput. Biol.* **12**, e1005167 (2016).
10. Peekhaus, N. & Conway, T. What's for dinner?: Entner–Doudoroff metabolism in *Escherichia coli*. *J. Bacteriol.* **180**, 3495–3502 (1998).
11. Mahadevan, R. & Lovley, D. R. The degree of redundancy in metabolic genes is linked to mode of metabolism. *Biophys. J.* **94**, 1216–1220 (2008).
12. Güell, O., Sagués, F. & Serrano, M. Á. Essential plasticity and redundancy of metabolism unveiled by synthetic lethality analysis. *PLoS Comput. Biol.* **10**, e1003637 (2014).
13. Nowak, M. A., Boerlijst, M. C., Cooke, J. & Smith, J. M. Evolution of genetic redundancy. *Nature* **388**, 167–171 (1997).
14. Murray, E. L. & Conway, T. Multiple regulators control expression of the Entner–Doudoroff aldolase (Eda) of *Escherichia coli*. *J. Bacteriol.* **187**, 991–1000 (2005).

15. Parisutham, V. & Lee, S. K. Novel functions and regulation of cryptic cellobiose operons in *Escherichia coli*. *PLoS ONE* **10**, e0131928 (2015).

16. Grüning, N. M. & Ralser, M. Glycolysis: how a 300yr long research journey that started with the desire to improve alcoholic beverages kept revolutionizing biochemistry. *Curr. Opin. Syst. Biol.* **28**, 100380 (2021).

17. Feist, A. M. et al. A genome-scale metabolic reconstruction for *Escherichia coli* K-12 MG1655 that accounts for 1260 ORFs and thermodynamic information. *Mol. Syst. Biol.* **3**, 121 (2007).

18. Fuhrman, L. K., Wanken, A., Nickerson, K. W. & Conway, T. Rapid accumulation of intracellular 2-keto-3-deoxy-6-phosphogluconate in an Entner–Doudoroff aldolase mutant results in bacteriostasis. *FEBS Microbiol. Lett.* **159**, 261–266 (1998).

19. Chantranupong, L., Wolfson, R. L. & Sabatini, D. M. Nutrient-sensing mechanisms across evolution. *Cell* **161**, 67–83 (2015).

20. Korem Kohanim, Y. et al. A bacterial growth law out of steady state. *Cell Rep.* **23**, 2891–2900 (2018).

21. Towbin, B. D. et al. Optimality and sub-optimality in a bacterial growth law. *Nat. Commun.* **8**, 14123 (2017).

22. Fischer, E. & Sauer, U. A novel metabolic cycle catalyzes glucose oxidation and anaplerosis in hungry *Escherichia coli*. *J. Biol. Chem.* **278**, 46446–46451 (2003).

23. Bren, A. et al. Glucose becomes one of the worst carbon sources for *E. coli* on poor nitrogen sources due to suboptimal levels of cAMP. *Sci. Rep.* **6**, 24834 (2016).

24. Taylor, B. R. et al. A metabolic sum rule dictates bacterial response to short-chain fatty acid stress. Preprint at *bioRxiv* https://doi.org/10.1101/2022.08.31.506075 (2022).

25. Hermsen, R., Okano, H., You, C., Werner, N. & Hwa, T. A growth-rate composition formula for the growth of *E. coli* on co-utilized carbon substrates. *Mol. Syst. Biol.* **11**, 801 (2015).

26. Xu, Y. F., Amador-Noguez, D., Reaves, M. L., Feng, X. J. & Rabinowitz, J. D. Ultrasensitive regulation of anapleurosis via allosteric activation of PEP carboxylase. *Nat. Chem. Biol.* **8**, 562–568 (2012).

27. Doucette, C. D., Schwab, D. J., Wingreen, N. S. & Rabinowitz, J. D. α-ketoglutarate coordinates carbon and nitrogen utilization via enzyme I inhibition. *Nat. Chem. Biol.* **7**, 894–901 (2011).

28. Kleijn, R. J., Van Winden, W. A., Van Gulik, W. M. & Heijnen, J. J. Revisiting the ^{13}C-label distribution of the non-oxidative branch of the pentose phosphate pathway based upon kinetic and genetic evidence. *FEBS J.* **272**, 4970–4982 (2005).

29. Stincone, A. et al. The return of metabolism: biochemistry and physiology of the pentose phosphate pathway. *Biol. Rev.* **90**, 927–963 (2015).

30. Pereira, F. C. & Berry, D. Microbial nutrient niches in the gut. *Environ. Microbiol.* **19**, 1366–1378 (2017).

31. Lenski, R. E., Rose, M. R., Simpson, S. C. & Tadler, S. C. Long-term experimental evolution in *Escherichia coli*. I. Adaptation and divergence during 2,000 generations. *Am. Nat.* **138**, 1315–1341 (1991).

32. Wünsche, A. et al. Diminishing-returns epistasis decreases adaptability along an evolutionary trajectory. *Nat. Ecol. Evol.* **1**, 61 (2017).

33. Lenski, R. E. Experimental evolution and the dynamics of adaptation and genome evolution in microbial populations. *ISME J.* **11**, 2181–2194 (2017).

34. Emmerling, M. et al. Metabolic flux responses to pyruvate kinase knockout in *Escherichia coli*. *J. Bacteriol.* **184**, 152–164 (2002).

35. Burgos-Barragan, G. et al. Mammals divert endogenous genotoxic formaldehyde into one-carbon metabolism. *Nature* **548**, 549–554 (2017).

36. Tibbetts, A. S. & Appling, D. R. Compartmentalization of mammalian folate-mediated one-carbon metabolism. *Annu. Rev. Nutr.* **30**, 57–81 (2010).

37. Corbet, C. & Feron, O. Cancer cell metabolism and mitochondria: nutrient plasticity for TCA cycle fueling. *Biochim. Biophys. Acta Rev. Cancer* **1868**, 7–15 (2017).

38. Kiparissides, A. & Hatzimanikatis, V. Thermodynamics-based metabolite sensitivity analysis in metabolic networks. *Metab. Eng.* **39**, 117–127 (2017).

39. Kee, J. M., Oslund, R. C., Perlman, D. H. & Muir, T. W. A pan-specific antibody for direct detection of protein histidine phosphorylation. *Nat. Chem. Biol.* **9**, 416–421 (2013).

40. Nguyen, J. et al. A distinct growth physiology enhances bacterial growth under rapid nutrient fluctuations. *Nat. Commun.* **12**, 3662 (2021).

41. Sekar, K. et al. Bacterial glycogen provides short-term benefits in changing environments. *Appl. Environ. Microbiol.* **86**, e00049–20 (2020).

42. Jenior, M. L., Moutinho, T. J., Dougherty, B. V. & Papin, J. A. Transcriptome-guided parsimonious flux analysis improves predictions with metabolic networks in complex environments. *PLoS Comput. Biol.* **16**, e1007099 (2020).

43. Wang, C. Y. et al. Metabolome and proteome analyses reveal transcriptional misregulation in glycolysis of engineered *E. coli*. *Nat. Commun.* **12**, 4929 (2021).

44. Yan, Y., Liu, N. & Tang, Y. Recent developments in self-resistance gene directed natural product discovery. *Nat. Prod. Rep.* **37**, 879–892 (2020).

45. Almabruk, K. H., Dinh, L. K. & Philmus, B. Self-resistance of natural product producers: past, present, and future focusing on self-resistant protein variants. *ACS Chem. Biol.* **13**, 1426–1437 (2018).

46. Hofmeyr, J. H. S. & Cornish-Bowden, A. Quantitative assessment of regulation in metabolic systems. *Eur. J. Biochem.* **200**, 223–236 (1991).

47. Kochanowski, K. et al. Global coordination of metabolic pathways in *Escherichia coli* by active and passive regulation. *Mol. Syst. Biol.* **17**, e10064 (2021).

48. Vander Heiden, M. G. et al. Evidence for an alternative glycolytic pathway in rapidly proliferating cells. *Science* **329**, 1492–1499 (2010).

Methods

Strains and culture conditions

E. coli K-12 strain NCM3722 was the WT in this study. The ED pathway knockout strains Δ*edd* and Δ*eda* with the NCM3722 background were produced by P1 phage transduction[49] of a deletion allele from the Keio collection[50]. *E. coli* were grown in Gutnick minimal (Gmin) media[51] at 37 °C. Media contained 0.2% (w/v) glucose, 0.274% (w/v) sodium acetate, 0.2% (w/v) mannose, 0.162% (v/v) glycerol or 0.45% (w/v) sodium succinate dibasic hexahydrate as the carbon source such that the same molar availability of elemental carbon was achieved. For the nitrogen source, media contained 10 mM NH_4Cl for the nitrogen-replete condition and either 2 mM NH_4Cl or 2.5 mM of arginine for the nitrogen-limited conditions. Culture density (OD_{600}) was monitored by spectrophotometer or plate reader.

For carbon upshift, cells were initially grown on acetate, mannose, succinate or glycerol. When cultures reached the mid-log phase of growth ($OD_{600} \approx 0.3$), carbon upshift was performed by spiking in a concentrated glucose or succinate stock solution into the culture to a final glucose concentration of 0.2% (w/v) or 0.45% (w/v) sodium succinate dibasic hexahydrate. For nitrogen upshift, cells were initially cultured in media containing 2 mM NH_4Cl or 2.5 mM arginine until mid-log phase. At $OD_{600} \approx 0.3$, cells consumed most of the nitrogen from NH_4Cl, slowing down cell growth, and arginine cultures were in the mid-log phase. To induce upshift, NH_4Cl was spiked into cultures to a final concentration of 10 mM. Metabolism was quenched and metabolites were extracted immediately before upshift (0 minutes) as well as 3, 5, 10 and 30 minutes after upshift. For isotope labeling experiments, unlabeled glucose was replaced with $[1,2^{-13}C_2]$-glucose, $[5,6^{-13}C_2]$-glucose or $[U^{-13}C_6]$-glucose.

LTEE strains REL606 (ancestral), REL2175A (Ara+3, 5,000 generations), REL2177A (Ara+5, 5,000 generations), REL2180A (Ara−2, 5,000 generations), REL11345 (Ara+3, 50,000 generations), REL11367 (Ara+5, 50,000 generations) and REL11333 (Ara−2, 50,000 generations) were used for this study. Cultures were grown in Davis Minimal (DM) broth as in the original LTEE, with the same carbon sources and upshifts described above. For no-carbon-to-glucose upshift, cells were inoculated into 0.02% (w/v) glucose limited media and allowed to reach the stationary phase for more than 4 h before upshifting by the addition of glucose. This timespan was chosen to reflect the LTEE conditions, in which cells starve for hours before their next dilution with glucose upshift.

Flux balance analysis of single gene glycolysis knockouts

Flux balance analysis was performed using the COnstraint-Based Reconstruction and Analysis Toolbox (COBRA) on MATLAB with the *E. coli* genome-scale reconstruction iAF1260 (ref. [52]). The objective function was set to maximize biomass production while satisfying the mass balance constraints and carbon uptake rates specified by:

$$S\mathbf{v} = 0$$

$$\mathbf{lb} \leq \mathbf{v} \leq \mathbf{ub}$$

S is the stoichiometric matrix, and **v** is the vector corresponding to reaction fluxes. **lb** and **ub** are the lower and upper bounds of **v** based on biochemical and thermodynamic considerations. Individual genes of the EMP or ED glycolysis were silenced by constraining the respective reaction's flux bounds to 0 mmol $gDCW^{-1} h^{-1}$. For simulations of growth on glucose, the glucose uptake rate was set to 8 mmol $gDCW^{-1} h^{-1}$ to reflect typical substrate uptake rates[52].

Nutrient upshift growth assays

To measure growth rates and accelerations during nutrient upshift, cells were grown in 96-well plates in a plate reader (BioTek) with shaking at 37 °C. Culture density (OD_{600}) was measured every 2 min. Growth

acceleration was computed as the time derivative of the specific growth rate (μ), which is the time derivative of log culture density ($\ln(C)$):

$$growth\ acceleration(a) = \frac{d\mu}{dt} = \frac{d^2 \ln(C)}{dt^2}$$

The maximum growth acceleration was quantified for acetate-to-glucose carbon upshift and ammonia depletion-to-repletion nitrogen upshift in the first 6 minutes and for arginine-to-ammonia nitrogen upshift and acetate-to-succinate, succinate-to-glucose and glycerol-to-glucose carbon upshifts in the first 10 min.

Intermittent nutrient upshift growth curves were performed by culturing cells in a 96-well plate in the plate reader. Cultures were first inoculated into plates with either glucose-depleted or NH_4Cl-depleted media before 0.02% (w/v) glucose or 0.5 mM NH_4Cl was added at $t = 0$ min. Upshift was monitored until the limiting nutrient was depleted and cell growth ceased for no longer than 15 min. For nutrient upshift, the plate was taken out from the plate reader for spiking in 0.02% (w/v) glucose or 0.5 mM NH_4Cl. These nutrient spike-in and growth monitoring steps were repeated a few times. All growth assays involving NCM3722 strains were performed in biological triplicates originating from three different colonies and, for each biological replicate, 12 technical replicates. To infer the population mean from the sample mean, s.e.m. using $n = 3$ biological replicates, in which each biological replicate was represented by the median of the technical replicates, was used. The growth assays for the LTEE strains were initially carried out the same as the ones for the NCM3722 strains. In subsequent growth assays, the number of biological replicates needed for a desired power of 0.8 ($\beta = 0.2$) and significance level ($\alpha = 0.05$) was determined through a power analysis with the measured means and variances from the initial assays (Extended Data Fig. 8e). For the LTEE strain growth assays with large numbers of biological replicates, no technical replicates were used. In all cases, each colony begot one biological replicate and one data point.

Metabolite extraction and measurement

Metabolite extraction was conducted as quickly as possible to minimize perturbations in metabolism. To quickly quench metabolism, remove extracellular metabolites and extract intracellular metabolites, 1 ml of cultures was vacuum-filtered onto nylon membrane filters (0.45 μm, Millipore) and flipped cell-side down into 400 μl of 40:40:20 high-performance liquid chromatography (HPLC)-grade acetonitrile:methanol:water that was pre-cooled to −20 °C in a six-well plate. Extraction continued at −20 °C for 20 minutes before the filter was flipped cell-side up and washed with the extraction solvent in the well. The extract was collected in an Eppendorf tube and centrifuged at 4 °C. The supernatant was dried under nitrogen flow and reconstituted in HPLC-grade water for LC−MS analysis.

The metabolite extract samples were analyzed by HPLC (Vanquish Duo UHPLC, Thermo Fisher Scientific) coupled to a high-resolution orbitrap mass spectrometer (Q Exactive Plus, Thermo Fisher Scientific). The LC separation was achieved using a hydrophilic interaction chromatography column (XBridge BEH Amide XP Column, 130 Å, 2.5 μm, 2.1 mm × 150 mm, Waters). MS was performed in both positive and negative mode using a mass resolution of 140,000 at 200 m/z. The resulting LC−MS data were processed using the Metabolomic Analysis and Visualization Engine (MAVEN)[53] with peaks identified by both the known retention times and mass-to-charge ratios (m/z)[54].

For LC−MS/MS analysis of valine, the same LC method was used with a modified MS protocol with a full MS/data-dependent MS^2 scan using a normalized collision energy (NCE) of 35. The positive parent ions of all valine isotopologues were inputted for MS^2 fragmentation. The resulting LC−MS/MS data were analyzed on MAVEN by first identifying the parent m/z for each valine isotopologue and then extracting its fragment spectra[53]. The use of valine for determination of the EMP

pathway, the ED pathway and the PPP fluxes assumes the source of measured valine being mainly de novo synthesis. Extracellular valine, if it is in high concentrations, and valine from protein degradation, if protein degradation flux is high, may affect our intracellular flux ratio measurement. The combination of rapid culture filtration method and an orthogonal approach (for example, 3PG labeling measurement) mitigates the risk of the misattribution of metabolic fluxes.

Quantitation of Gibbs free energy of reaction

Absolute metabolite concentrations in different conditions and time-points were obtained by comparing peak areas to the known reference points in which the absolute concentrations of central carbon metabolites of *E. coli* had been measured[55,56]. The KDPG concentration was measured using an isotope-ratio-based approach[57]. Cellular metabolites were labeled by culturing *E. coli* on [U-^{13}C$_6$]-glucose for multiple generations and extracted using the extraction solvent containing known concentrations of the unlabeled KDPG internal standard.

Using absolute metabolite concentrations (Supplementary Table 1), Gibbs free energy of reaction (ΔG) was computed using the following equation:

$$\Delta G = \Delta G'^{\circ} + RT \ln Q$$

$\Delta G'^{\circ}$ is ΔG at standard biochemical conditions; R is the universal gas constant; T is the temperature in kelvins; and Q is the reaction quotient (that is, the ratio of product-to-substrate activities, which are effective concentrations in a non-ideal solution). ΔG and changes in ΔG from one state to another ($\Delta\Delta G$) were computed for the EMP pathway, the ED pathway and gluconeogenesis (Supplementary Note 1).

Cell lysate assay

Measurement of the ED pathway activity in acetate cultures was conducted by monitoring KDPG production from cell lysates upon adding 6PG. Cells were grown on acetate until cultures reached ~0.4 OD$_{600}$. Cells were pelleted, washed twice in cold PBS and resuspended in PBS. Cells were lysed by addition of 20 mg ml^{-1} lysozyme and sonication before subsequent centrifugation for 10 min. All lysis steps were conducted at 4 °C. The supernatant was moved to an Eppendorf tube and heated to 37 °C. Then, 5 mM 6PG was added to the cell lysate and the reaction mixture was incubated at 37 °C with continuous shaking. Small aliquots of the reaction mixture were sampled over time. The reaction in those aliquots was quenched by the addition of cold 40:40:20 methanol:acetonitrile:water at a 1:4 ratio of the aliquot to the quenching solution. The mixture was centrifuged, and the supernatant was taken for the measurement of KDPG by LC–MS.

Glycolytic pathway flux quantitation via labeling in lower glycolysis metabolites

Glycolytic fluxes were obtained using the intracellular metabolite labeling from [1,2-^{13}C$_2$]-glucose, [5,6-^{13}C$_2$]-glucose or [U-^{13}C$_6$]-glucose tracers (Supplementary Tables 2–10). [1,2-^{13}C$_2$]-glucose and [5,6-^{13}C$_2$]-glucose tracers provided the necessary metabolite labeling (for example, 3PG, 6PG and valine) for determination of central carbon metabolism fluxes (Supplementary Notes 2 and 3). For the carbon upshift case, [U-^{13}C$_6$]-glucose tracer provided information necessary to correct for incomplete turnover of 3PG in early timepoints (Supplementary Note 4). In brief, because the isotope labeling of 3PG from [1,2-^{13}C$_2$]-glucose depends on which route glucose took (the EMP pathway, ED pathway or PPP), the following relationships between pathway fluxes and 3PG isotopologues were derived with the model shown in Supplementary Note 3.

$$3PG_{M+0} = \frac{v_{EMP} + v_{ED} + v_{PPP}}{Q}$$

$$3PG_{M+1} = \frac{\frac{1}{3}v_{PPP}}{Q}$$

$$3PG_{M+2} = \frac{v_{EMP} + \frac{1}{3}v_{PPP}}{Q}$$

Q is the normalization factor that ensures that the sum of 3PG mass isotopomer fractions is 1. These equations were rearranged to solve for the ED-to-EMP flux ratios in Fig. 5:

$$\frac{v_{ED}}{v_{EMP}} = \frac{3PG_{M+0} - 3PG_{M+2} - 2 \times 3PG_{M+1}}{3PG_{M+2} - 3PG_{M+1}}$$

Measurement of instantaneous glucose uptake rates

To measure glucose uptake rates (that is, total glycolytic fluxes) in dynamic states, the instantaneous accumulation of a glucose-6-phosphate (G6P) analogue 2-deoxyglucose-6-phosphate (2DGP) was quantified using LC–MS upon feeding 2-deoxyglucose (2DG) for 5 seconds. At 5 seconds before each collection timepoint in nutrient upshift experiments, a 1-ml aliquot of the culture was rapidly mixed with 10 μl of 2DG solution in a pre-warmed 1.5-ml tube before subsequent metabolite extraction. The concentration of 2DG was chosen to achieve a final glucose-to-2DG ratio between 1 and 5 and an intracellular 2DGP concentration of 10 mM or less. The absolute glucose uptake rates were obtained by comparing the 2DGP peak areas in samples to those of steady-state conditions with previously measured rates:

$$R = R_{ref} \times \frac{P}{P_{ref}} \times \frac{F_{ref}}{F}$$

R denotes the glucose uptake rate (mmol gCDW^{-1} h^{-1}); P denotes the 2DGP peak area normalized to the culture density; and F denotes the fraction of 2DG over the sum of glucose and 2DG. P_{ref} and F_{ref} are the values from the 2DG spike-in experiments using the cells in reference steady-state conditions with known R (R_{ref}).

Flow cytometry of WT-Δedd co-cultures

WT and Δedd strains were transformed with plasmids modified from pZE27GFP (Addgene, 75452) to carry an ampicillin selection marker and either GFP or mCherry, respectively. To generate co-cultures, the overnight cultures of WT and Δedd strains were resuspended in ratios of 1:1, 2:1 and 1:2 to a final OD$_{600}$ of ~0.06 in 12-well plates in media containing low glucose (0.02%, w/v) or low ammonia (0.5 mM NH$_4$Cl) and 50 μg ml^{-1} ampicillin. Nutrient upshifts were performed as described above, and, at the end of each upshift cycle, 200 μl of the culture was collected and resuspended in cold Gmin buffer without any carbon or nitrogen to an OD of ~0.1. Samples were run (BD LSRII Flow Cytometer, BD Biosciences) with WT+GFP and Δedd+mCherry as well as WT−GFP and Δedd−mCherry controls used for compensation. Data were analyzed on FlowJo 10.8.2 with the gating strategy illustrated in Extended Data Fig. 6.

Analysis of the LTEE

The LTEE encompassed six cultures from each of the ancestral strains REL606 and REL607 (12 cultures total) in a DM medium with 25 mg L^{-1} glucose (citrate was also included in this medium as a chelating agent, which the ancestral strain does not grow on). Cultures were diluted 1:100 into the fresh medium daily, and two clones from each culture were sampled periodically for sequencing. The mutation history of the 12 populations was downloaded from https://barricklab.org/shiny/LTEE-Ecoli/ and analyzed using MATLAB and Python programs. Non-synonymous (missense and nonsense) mutations and indels were considered for all analyses, and synonymous mutations were also included where stated (for example, Extended Data Figs. 7 and 8b).

The mutation history of the ED and EMP pathways were compared to other pathways. Because the assignment of genes to metabolic pathways is not always one-to-one or clear-cut, pseudo pathways were formed from randomly generated groups of genes. Each pseudo pathway was generated by randomly selecting 10 genes from the *E. coli* genome. Mutations in the pathway genes were counted and normalized by the number of genes in the pathway at each generation. This process was repeated for 1,000 pathways as well as the EMP and ED pathways, and the percentile ranks of the EMP and ED pathways' per-gene mutations were obtained. The EMP and ED pathways included the following mutually exclusive sets of glycolytic genes: *pgi*, *pfka*, *pfkb*, *fbaa*, *fbab* and *tpia* were included in the EMP pathway, and *zwf*, *pgl*, *edd* and *eda* were included in the ED pathway. These gene sets were also used to track the number of strains with mutations in the EMP and ED pathways.

To assess the randomness of the mutation history, mutation data from generation 50,000 were compared to the Poisson distribution. Without considering their identity, individual genes' mutations were counted for all 24 clones. Because each of the populations begot two clones, which are, thus, not independent of each other, 2^{12} sets of 12 independent clones were generated using only one of the two sequenced clones from each population. Each set generated a distribution of frequencies of mutations in a gene. The mean and s.d. of these distributions over the 2^{12} sets were obtained. The resulting distribution was fit to a Poisson distribution using the MATLAB curve fitting toolbox (Extended Data Fig. 7a,b).

Reporting summary

Further information on research design is available in the Nature Portfolio Reporting Summary linked to this article.

Data availability

Source data for Figs. 1–6 are provided in Supplementary Tables 1–17 and the GitHub public repository: https://github.com/richardlaw517/Parallel_Glycolysis.
LTEE source data are available at https://barricklab.org/shiny/LTEE-Ecoli/. Source data are provided with this paper.

Code availability

The code for the analysis of metabolic fluxes and LTEE is available on the GitHub public repository: https://github.com/richardlaw517/Parallel_Glycolysis.

References

49. Saragliadis, A., Trunk, T. & Leo, J. C. Producing gene deletions in *Escherichia coli* by P1 transduction with excisable antibiotic resistance cassettes. *J. Vis. Exp.* **2018**, 58267 (2018).
50. Baba, T. et al. Construction of *Escherichia coli* K-12 in-frame, single-gene knockout mutants: the Keio collection. *Mol. Syst. Biol.* **2**, 2006.0008 (2006).
51. Gutnick, D., Calvo, J. M., Klopotowski, T. & Ames, B. N. Compounds which serve as the sole source of carbon or nitrogen for *Salmonella typhimurium* LT-2. *J. Bacteriol.* **100**, 215–219 (1969).
52. Orth, J. D. et al. A comprehensive genome-scale reconstruction of *Escherichia coli* metabolism—2011. *Mol. Syst. Biol.* **7**, 535 (2011).
53. Seitzer, P., Bennett, B. & Melamud, E. MAVEN2: an updated open-source mass spectrometry exploration platform. *Metabolites* **12**, 684 (2022).
54. Wang, L. et al. Peak annotation and verification engine for untargeted LC–MS metabolomics. *Anal. Chem.* **91**, 1838–1846 (2019).
55. Yuan, J. et al. Metabolomics-driven quantitative analysis of ammonia assimilation in *E. coli*. *Mol. Syst. Biol.* **5**, 302 (2009).
56. Park, J. O. et al. Metabolite concentrations, fluxes and free energies imply efficient enzyme usage. *Nat. Chem. Biol.* **12**, 482–489 (2016).
57. Bennett, B. D., Yuan, J., Kimball, E. H. & Rabinowitz, J. D. Absolute quantitation of intracellular metabolite concentrations by an isotope ratio-based approach. *Nat. Protoc.* **3**, 1299–1311 (2008).

Acknowledgements

Author contributions

Competing interests

The authors declare no competing interests.

Additional information

a

b

c
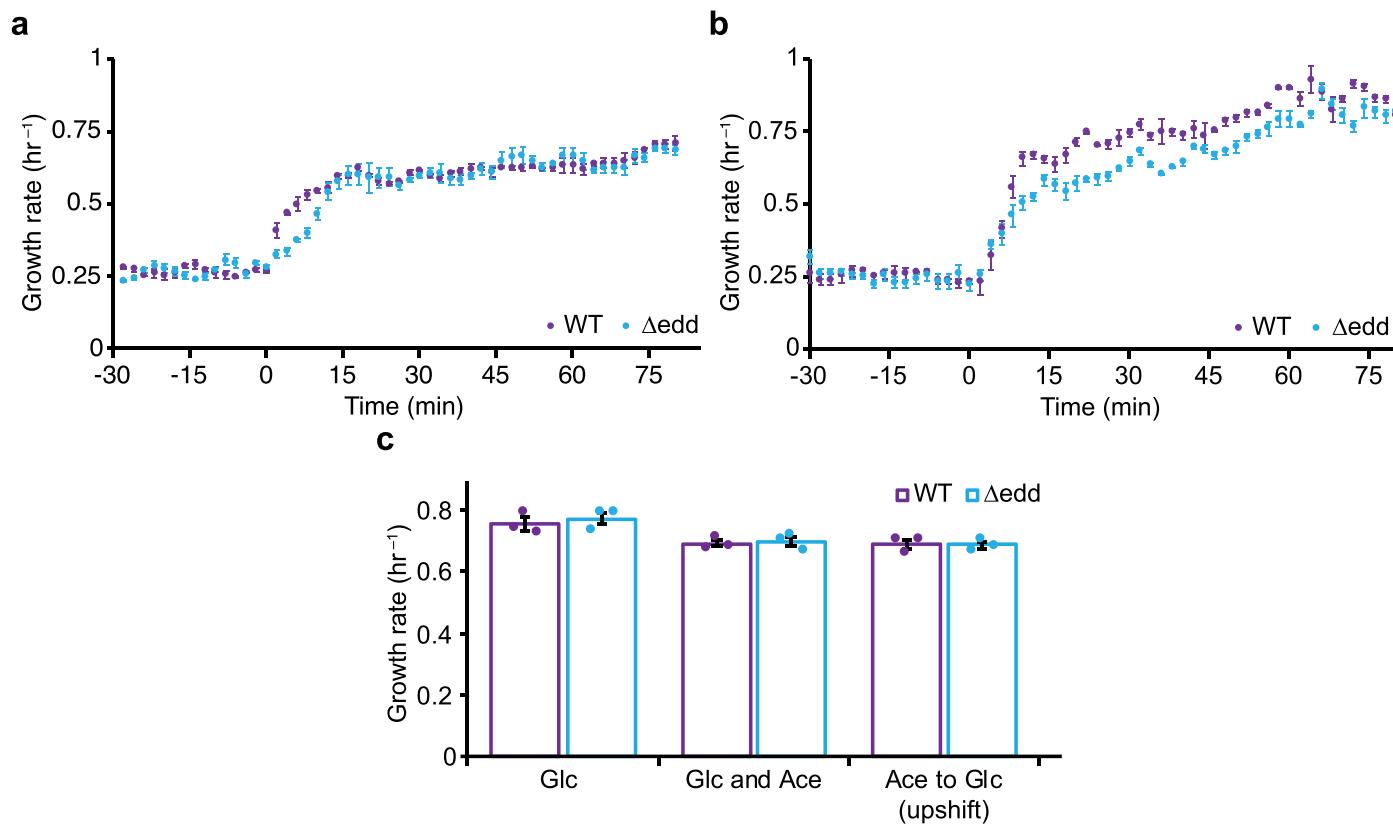
Extended Data Fig. 1 | Parallel glycolysis bolsters growth acceleration upon carbon and nitrogen upshifts. a, WT and Δ*edd* strains had been cultured on acetate as the sole carbon source and, at t = 0 min, were spiked with glucose. Growth rates were monitored until a steady growth rate of ~0.7 hr⁻¹ was achieved 80 minutes after upshift. **b**, WT and Δ*edd* strains were cultured on arginine as the sole nitrogen source before ammonia was spiked in at t = 0 min. Growth rates were monitored until a stable growth rate of ~0.75 hr⁻¹ was achieved. **c**, The growth rates of WT and Δ*edd* were measured in glucose minimal media with and without high acetate and compared to the stable growth rates of *E. coli* cultures following carbon upshift from acetate to glucose spiked in. Error bars represent the s.e.m. (n = 3 biological replicates).
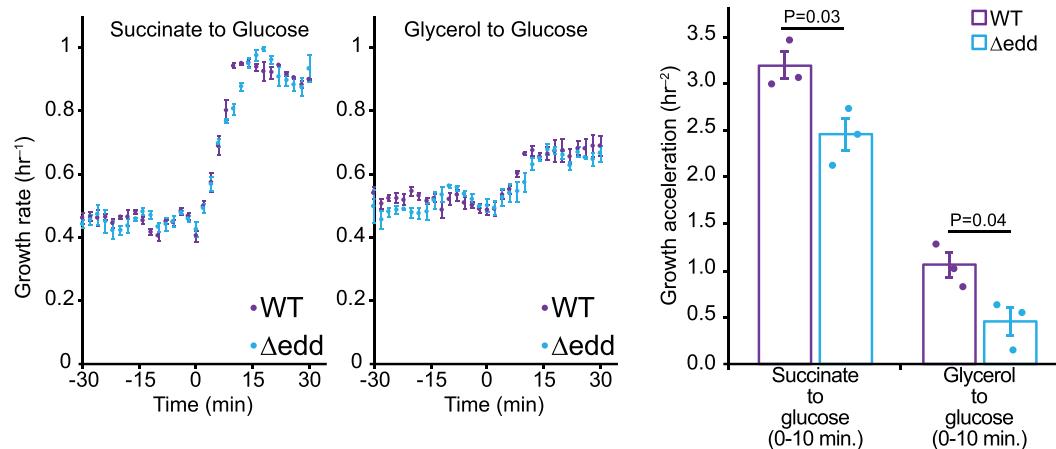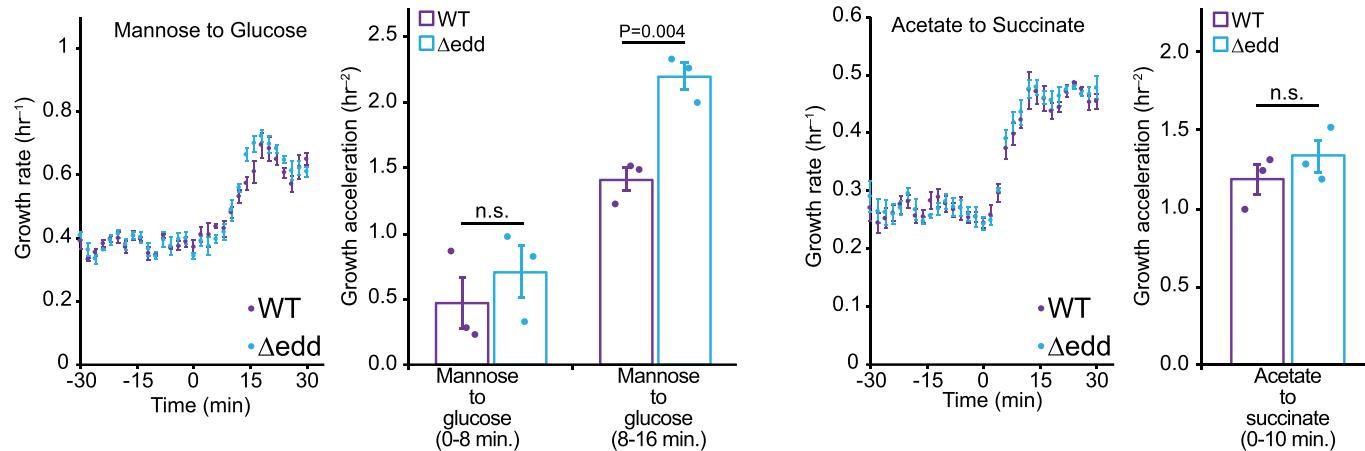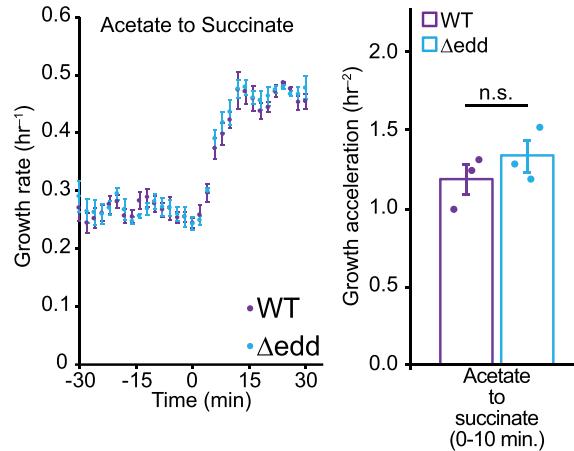
Extended Data Fig. 2 | The ED pathway improves growth acceleration upon carbon upshift from non-glycolytic to glycolytic substrates. a, WT and Δ*edd* cultures had been grown on succinate or glycerol as the sole carbon source and, at t = 0 min, were spiked with glucose. Growth rates and growth acceleration, which is the time derivative of growth rate, were quantified. **b**, Cells had been grown on a PTS sugar mannose as the sole carbon source and, at t = 0 min, were spiked with glucose. Growth rates as well as growth acceleration over two time periods were quantified. **c**, Cells were subjected to carbon upshift from acetate to succinate, both gluconeogenic substrates at t = 0 min. Growth rates and growth acceleration were quantified. Error bars represent the s.e.m. (n = 3 biological replicates). *P* values are obtained by two-tailed t-tests.
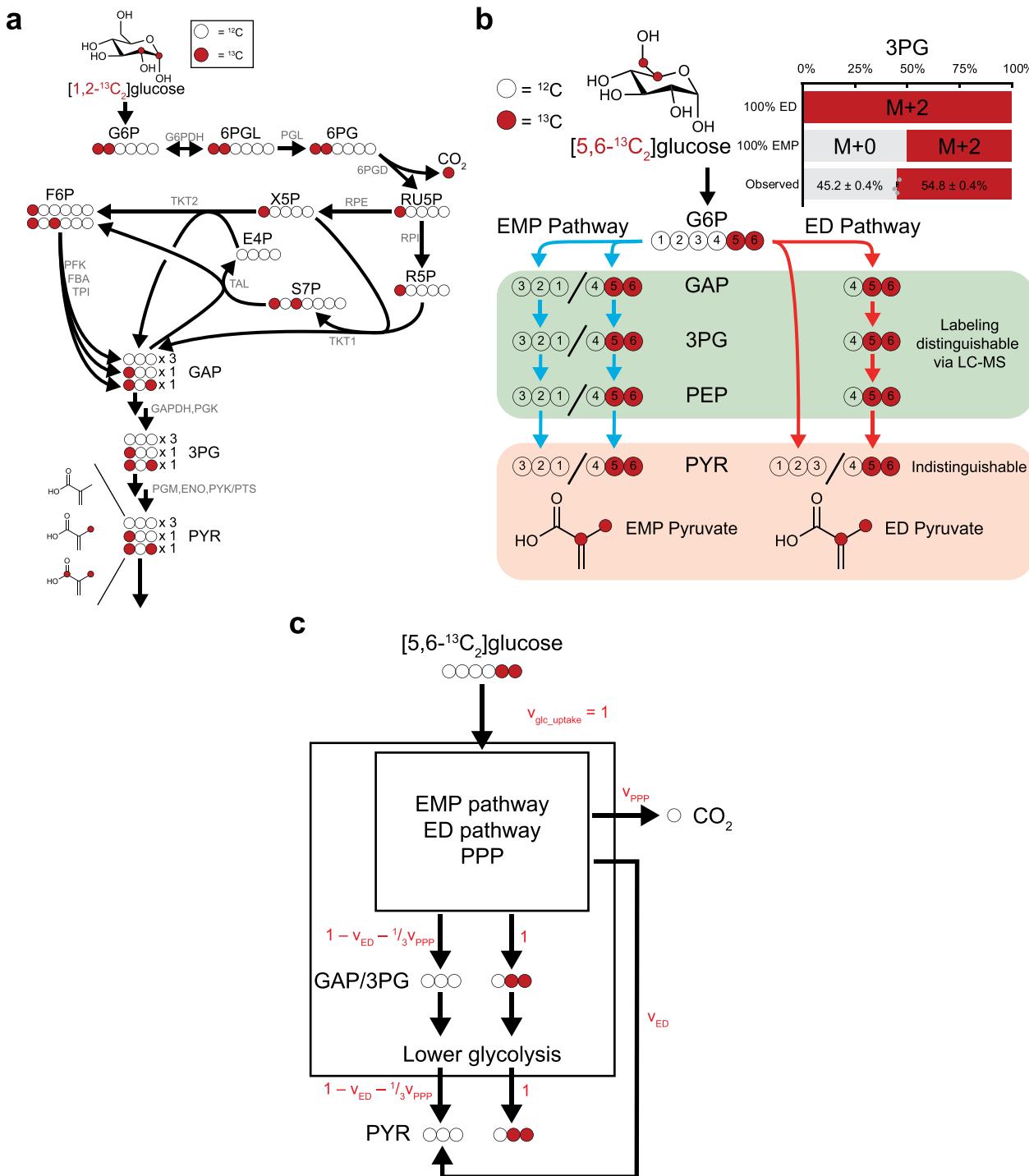
Extended Data Fig. 3 | [1,2-¹³C₂]- and [5,6-¹³C₂]-glucose reveal fluxes through different glycolytic routes. a, [1,2-¹³C₂]-glucose uniquely generates M + 1 labeled triose phosphates through the oxidative pentose phosphate pathway (OxPPP). For every three glucose molecules going through the PPP, three molecules of M + 0, one molecule of M + 1, and one molecule of M + 2 triose phosphate are generated. **b**, [5,6-¹³C₂]-glucose introduces unlabeled lower glycolytic intermediates only through the EMP pathway. Unlike in the case of [1,2-¹³C₂]-glucose, the EMP and the ED pathways produce the same positionally labeled pyruvate. The major fraction of M + 2 3PG indicated the ED pathway activity in

the nutrient replete condition. **c**, Using the carbon balance model of central carbon metabolism with [5,6-¹³C₂]-glucose, 3PG and pyruvate (PYR) labeling measurements are sufficient to solve for central carbon metabolism fluxes. This elegant solution is attributable to the fact that [5,6-¹³C₂]-glucose tracing is not convoluted by carbon shuffling in the PPP. Mass balance of carbons over the EMP pathway, the ED pathway, and the PPP (the inner control volume) as well as lower glycolysis (the outer control volumes) revealed the relationship between 3PG and PYR labeling and the central carbon metabolism fluxes.

a
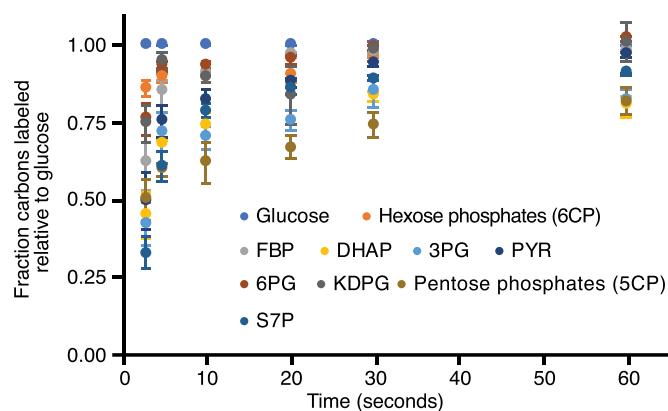
b
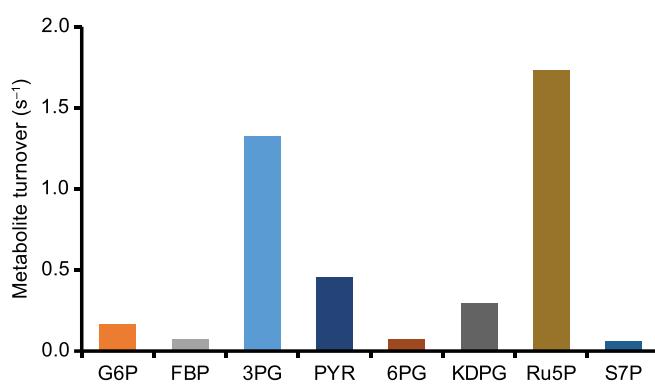
Extended Data Fig. 4 | Rapid labeling and turnover of glycolytic intermediates. a, *E. coli* grown on an unlabeled medium were rapidly switched to the same medium containing [U-^{13}C$_6$]-glucose. The labeled fractions of glycolytic intermediates were measured using LC-MS and normalized to the labeled fraction of glucose. Error bars represent the s.e.m. (n = 3 biological replicates). **b**, The turnover of individual metabolites was calculated as the flux through that metabolite divided by the metabolite pool size using previously reported fluxes and concentrations[56].
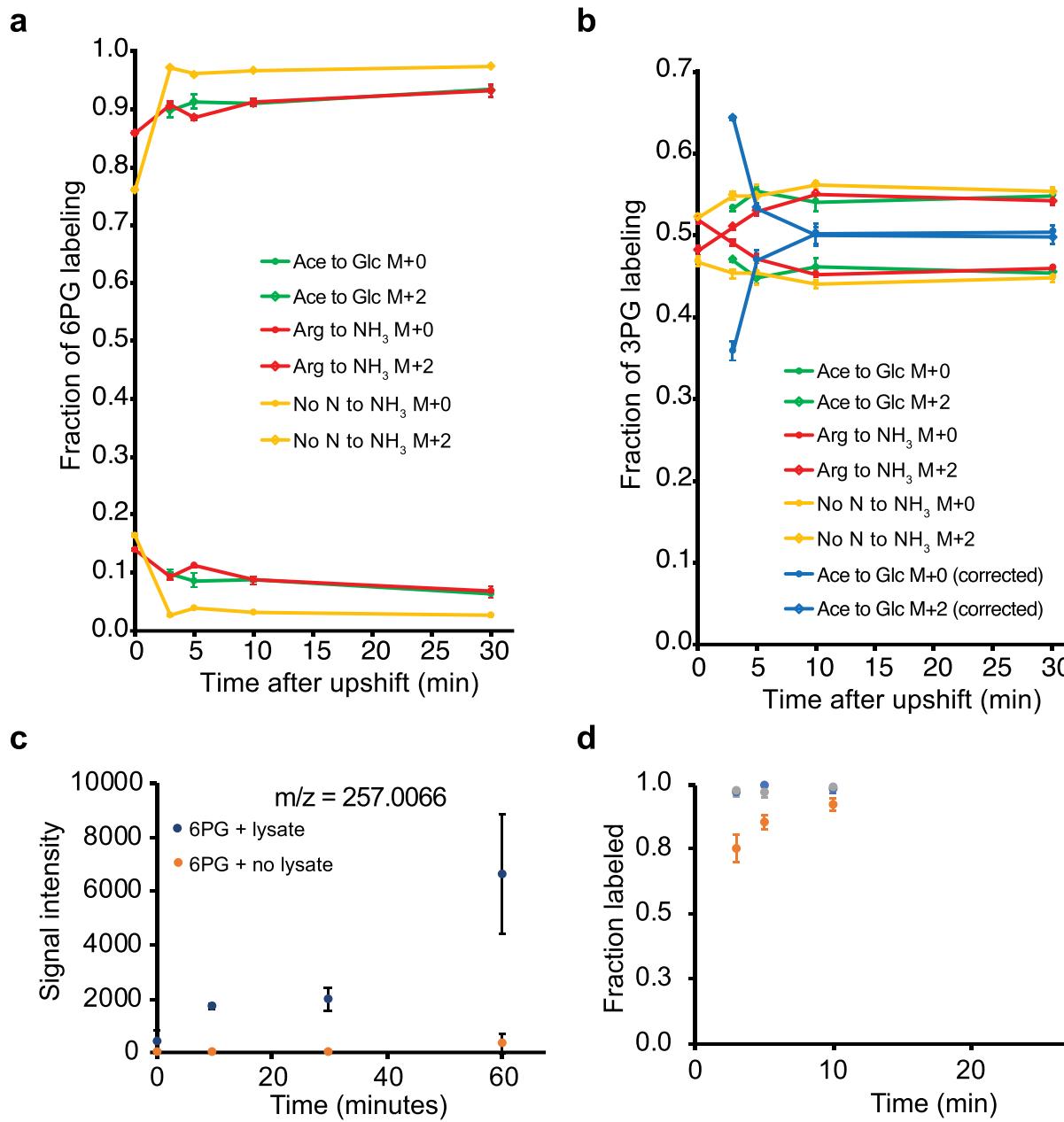
Extended Data Fig. 5 | The ED pathway flux jumps upon nutrient upshifts.
a,b, Nutrient upshift experiments analogous to those conducted with $[1,2\text{-}^{13}C_2]$-glucose were replicated using $[5,6\text{-}^{13}C_2]$-glucose and the resulting labeling of (**a**) 6PG and (**b**) 3PG was measured via LC-MS. The labeling of M + 0 and M + 2 isotopomers revealed both the ED pathway flux and recursive PPP usage (Supplementary Note 3). **c**, Cell lysates from *E. coli* cultures grown on acetate were collected for an enzyme activity assay and incubated with 6PG, the direct precursor to KDPG (m/z = 257.0066) in the ED pathway. The increase in KDPG

over time indicated the presence of the ED pathway enzymes in cells operating gluconeogenesis. Error bars represent the s.e.m. (n = 2 biological replicates). **d**, *E. coli* in the carbon-limited acetate medium underwent carbon upshift by $[U\text{-}^{13}C_6]$-glucose addition. The labeling of glycolytic intermediates following the upshift informed us of the fractions of 3PG pool coming from the labeled glucose and from the pre-upshift unlabeled acetate. This information was used to accurately compute glycolytic fluxes from $[1,2\text{-}^{13}C_2]$-glucose and $[5,6\text{-}^{13}C_2]$-glucose tracing. Error bars represent the s.e.m. (n = 3 biological replicates).
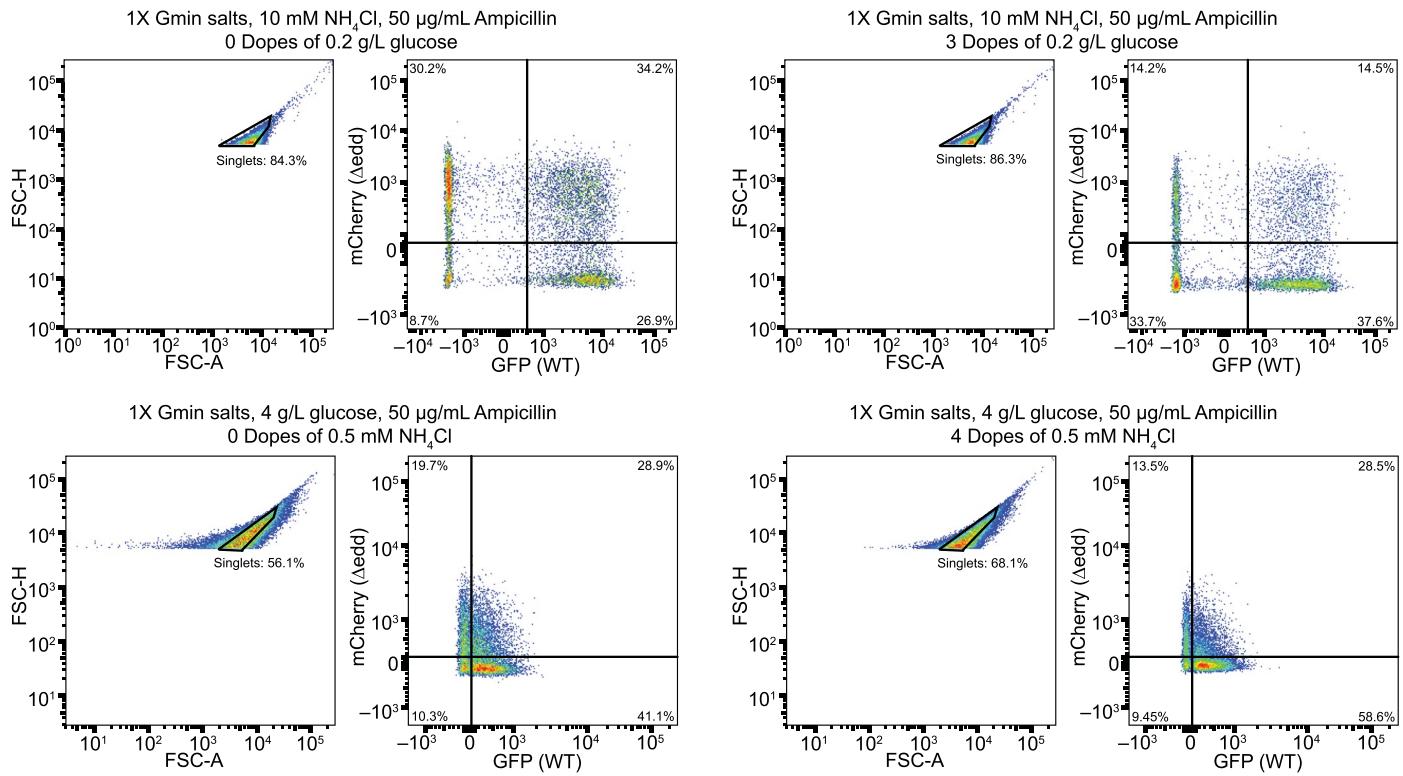
Extended Data Fig. 6 | Flow cytometry of WT-Δ*edd* co-cultures. At least 10,000 events were recorded per sample. Singlets were gated based on FSC-A (forward scattered area) and FSC-H (forward scatted height) intensities in a way to minimize the frequency of aggregates observed. Non-fluorescent (WT), GFP expressing (WT + GFP) and mCherry expressing (Δ*edd*+mCherry) cells were used as controls and analyzed on the day of experiments to determine the compensation of spectral overlap between fluorophores and gating quadrants for the glucose upshift (top) and ammonia upshift (bottom) experiments. Samples at the beginning (left) and end (right) of co-culture intermittent nutrient supply experiments are shown as examples.
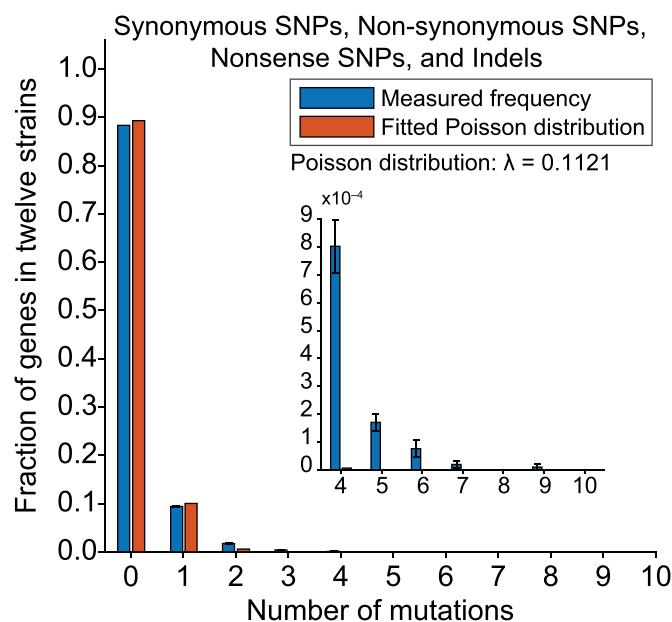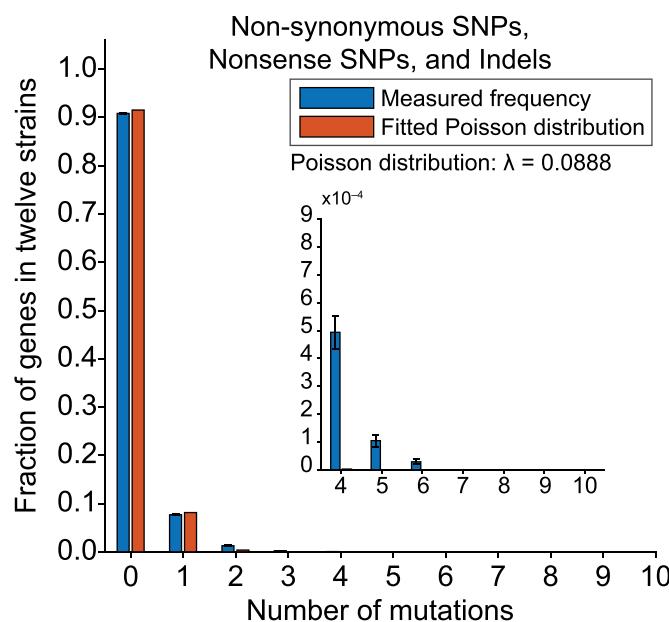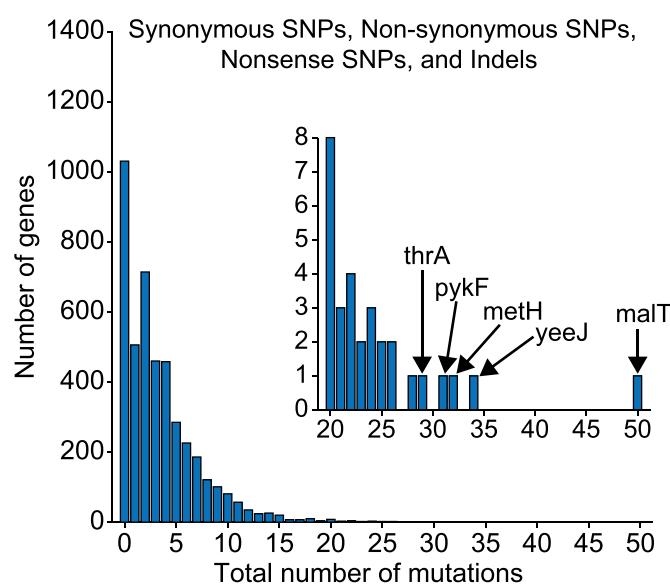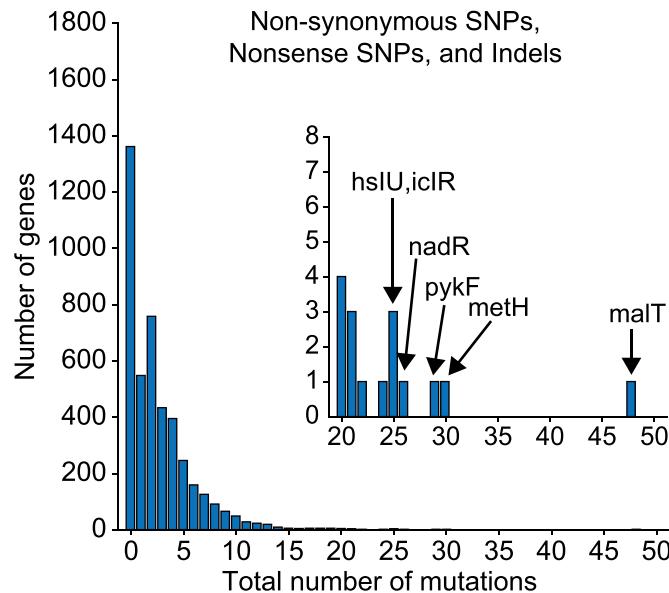
Extended Data Fig. 7 | Mutations in the LTEE reflect selective pressure.
a,b, Mutation frequencies in genes deviated from the Poisson distribution. Genes with the same number of mutations were counted, and the normalized counts were fit to a Poisson distribution. Poor fitting for genes with 2 or more mutations suggested a driving force toward improved fitness. Error bars represent the standard deviation (n = 2^{12} all possible sets of twelve independent clones). **c,d**, The total number of mutations in individual genes across all 24 strains at the 50,000th generation. For each gene, we counted the number of mutations

in all 24 strains. A few genes were consistently and heavily mutated: malT is a regulator for the maltose regulon that is also involved in λ phage infection; yeeJ is an autotransporter protein; metH is the gene for methionine synthase; pykF is pyruvate kinase, the last step of glycolysis; thrA is a bifunctional aspartokinase and homoserine dehydrogenase; nadR is a regulator for NAD biosynthesis; hsIU is a putative ATP dependent protease; and iclR is a regulator for isocitrate lyase of the glyoxylate cycle.

a

b

c

		EMP					ED			
	pgi	pfka	pfkb	fbaa	fbab	tpia	zwf	pgl	edd	eda
Ara-1 A		SNP								
Ara-1 B		SNP								
Ara-2 A			FS	SNP	SNP		SNP			
Ara-2 B										
Ara-3 A					2 SNP					
Ara-3 B					SNP					
Ara-4 A										
Ara-4 B										
Ara-5 A										
Ara-5 B										
Ara-6 A		SNP								
Ara-6 B										
Ara+1 A										
Ara+1 B										
Ara+2 A										
Ara+2 B										
Ara+3 A							SNP		SNP	
Ara+3 B							SNP		SNP	
Ara+4 A										
Ara+4 B										
Ara+5 A										
Ara+5 B										
Ara+6 A			SNP				SNP			
Ara+6 B	SNP				SNP					

Generation 50,000

d

e

No C to Glucose

Acetate to Glucose

Mannose to Glucose

Glycerol to Glucose

f

Acetate to Glucose

	Anc.	Ara+3	Ara+5	Ara-2
Generation	0	5,000	5,000	5,000
ED mutations	(None)	(1:*zwf*)	(None)	(None)
EMP mutations	(None)	(None)	(None)	(1:*fbaB*)
Total mutations	(None)	68	9	59

Extended Data Fig. 8 | Mutations in the EMP and the ED pathways over the LTEE improve growth acceleration. a, Development of nonsynonymous mutations and indels in randomly sampled gene groups were compared to the mutation history of the parallel glycolytic pathways over 50,000 generations of the *E. coli* long-term evolution experiment (LTEE). **b**, The proportions of nonsynonymous mutations and indels were monitored over the LTEE. **c**, List of mutations in the ED and the EMP pathways. The 24 genome sequences from 12 populations were analyzed at generation 50,000 for mutations in the two glycolytic pathways. SNP denotes a single nucleotide polymorphism (only nonsynonymous mutations are shown) and FS denotes a frameshift indel. **d**, Seven strains from the LTEE with different numbers of overall and ED-pathway mutations were chosen for growth assays. **e**, The LTEE strains underwent carbon

upshifts from no carbon source, acetate, mannose, or glycerol by spiking in glucose, and their growth acceleration was measured. Error bars represent the s.e.m. (n = 3 biological replicates). *P* values are obtained by two-tailed t-tests between the designated and ancestral strain. **f**, After power analysis, the ancestral strain and Ara+3 A, Ara+5 A, and Ara-2 A strains isolated in the 5,000[th] generation were subjected to acetate-to-glucose upshift, and their growth acceleration was measured. Each box shows the three quartiles, and whiskers extend to the minimum and maximum values within 1.5-fold of the interquartile range (n = 6 biological replicates). Statistical significance between strains was obtained by one-way ANOVA with Tukey's honestly significant difference test for multiple comparison.

a

	ED Pathway	PPP
Substrate	Glucose	
Carbon yield	100%	83.3%
NADPH yield	1	2

b

c

Extended Data Fig. 9 | The ED pathway provides dual benefits of carbon-efficient NADPH production and seamless nitrogen-controlled glucose import. a, The OxPPP produces two NADPH, but a carbon is lost as CO_2 as 6PG enters the non-oxidative pentose phosphate pathway. On the other hand, the ED pathway produces NADPH without decarboxylation. **b**, Exponentially growing *E. coli* in unlabeled glucose minimal medium were rapidly switched to either [1-$^2H_1$]- or [3-$^2H_2$]-glucose. Labeling of the hydride of NADPH from [1-$^2H_1$]-glucose indicated flux through G6PDH, whereas labeling from [3-$^2H_1$]-glucose indicated

flux through 6PGD. The ~3-fold labeling of NADPH from G6PDH compared to 6PGD indicated comparable contributions of the ED pathway and the OxPPP to NADPH generation. **c**, Concerted action of the phosphotransferase system (PTS), phosphoenolpyruvate synthase (PpsA), and ED pathway streamlines glucose import upon nitrogen upshift. While the EMP pathway takes 8 steps to generate PEP for glucose import, the concerted regulation and action of the ED pathway and PpsA supply PEP in 5 steps.

Corresponding author(s): Junyoung Park

Last updated by author(s): Jun 26, 2023
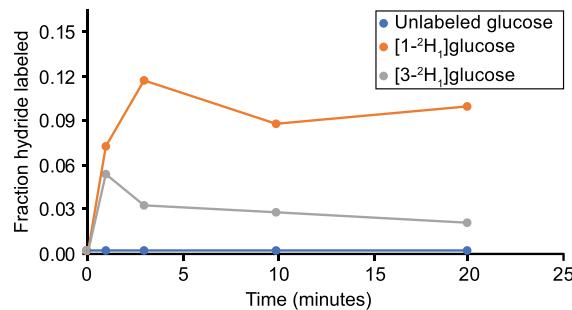
Reporting Summary

Nature Portfolio wishes to improve the reproducibility of the work that we publish. This form provides structure for consistency and transparency in reporting. For further information on Nature Portfolio policies, see our Editorial Policies and the Editorial Policy Checklist.

Statistics

For all statistical analyses, confirm that the following items are present in the figure legend, table legend, main text, or Methods section.

n/a	Confirmed	
☐	☒	The exact sample size (*n*) for each experimental group/condition, given as a discrete number and unit of measurement
☐	☒	A statement on whether measurements were taken from distinct samples or whether the same sample was measured repeatedly
☐	☒	The statistical test(s) used AND whether they are one- or two-sided *Only common tests should be described solely by name; describe more complex techniques in the Methods section.*
☒	☐	A description of all covariates tested
☐	☒	A description of any assumptions or corrections, such as tests of normality and adjustment for multiple comparisons
☐	☒	A full description of the statistical parameters including central tendency (e.g. means) or other basic estimates (e.g. regression coefficient) AND variation (e.g. standard deviation) or associated estimates of uncertainty (e.g. confidence intervals)
☐	☒	For null hypothesis testing, the test statistic (e.g. *F*, *t*, *r*) with confidence intervals, effect sizes, degrees of freedom and *P* value noted *Give P values as exact values whenever suitable.*
☒	☐	For Bayesian analysis, information on the choice of priors and Markov chain Monte Carlo settings
☒	☐	For hierarchical and complex designs, identification of the appropriate level for tests and full reporting of outcomes
☒	☐	Estimates of effect sizes (e.g. Cohen's *d*, Pearson's *r*), indicating how they were calculated

Our web collection on statistics for biologists contains articles on many of the points above.

Software and code

Policy information about availability of computer code

Data collection	Software: Xcalibur by Thermo Scientific (https://www.thermofisher.com/order/catalog/product/OPTON-30965), BD FACSDiva by BD Biosciences (https://www.bdbiosciences.com/en-us/products/software/instrument-software/bd-facsdiva-software)
Data analysis	Software: Maven (http://genomics-pubs.princeton.edu/mzroll/index.php) v2.0.0, Microsoft Excel v16.74, FlowJo v10.8.2, Python v3.10, R v4.3.0, RStudio 2023.03.0, and Matlab v2022a. The code for the analysis of metabolic fluxes and long-term evolution experiment is available on the GitHub public repository: https://github.com/richardlaw517/Parallel_Glycolysis

For manuscripts utilizing custom algorithms or software that are central to the research but not yet described in published literature, software must be made available to editors and reviewers. We strongly encourage code deposition in a community repository (e.g. GitHub). See the Nature Portfolio guidelines for submitting code & software for further information.

Data

Policy information about availability of data

All manuscripts must include a data availability statement. This statement should provide the following information, where applicable:
- Accession codes, unique identifiers, or web links for publicly available datasets
- A description of any restrictions on data availability
- For clinical datasets or third party data, please ensure that the statement adheres to our policy

Source data for Figures 1-6 and Extended Data Figures 1-10 are provided in the Source Files, Supplementary Tables 1-17 and the GitHub public repository: https://github.com/richardlaw517/Parallel_Glycolysis
LTEE source data is available on https://barricklab.org/shiny/LTEE-Ecoli/

Human research participants

Policy information about studies involving human research participants and Sex and Gender in Research.

Reporting on sex and gender	N/A
Population characteristics	N/A
Recruitment	N/A
Ethics oversight	N/A

Note that full information on the approval of the study protocol must also be provided in the manuscript.

Field-specific reporting

Please select the one below that is the best fit for your research. If you are not sure, read the appropriate sections before making your selection.

☒ Life sciences   ☐ Behavioural & social sciences   ☐ Ecological, evolutionary & environmental sciences

For a reference copy of the document with all sections, see nature.com/documents/nr-reporting-summary-flat.pdf

Life sciences study design

All studies must disclose on these points even when the disclosure is negative.

Sample size	Data were taken from at least three biological replicates. The sample size was chosen for microbial culture experiments because microbial experiments are well-controlled and three replicates are typically sufficient. For strains from the long-term evolution experiment, sample sizes to test differences in growth acceleration were obtained by power analysis with desired power of 0.80 and alpha of 0.05 from the mean and variance of a pilot study of three biological replicates.
Data exclusions	No data were excluded.
Replication	All attempts at replication were successful. All key experiments were performed independently on separate days.
Randomization	LC-MS samples were analyzed in random order. For cell culture, single colonies of strains were selected at random to initiate the cultures. As groups of single colonies were randomly chosen from individual agar plates of different strains, no covariates were relevant or used.
Blinding	The investigators were not blinded to the group allocation during data collection or analysis. Blinding was not necessary since measurements did not involve bias from the experimentalist. All data were processed using the same software and code.

Reporting for specific materials, systems and methods

We require information from authors about some types of materials, experimental systems and methods used in many studies. Here, indicate whether each material, system or method listed is relevant to your study. If you are not sure if a list item applies to your research, read the appropriate section before selecting a response.

Materials & experimental systems

n/a	Involved in the study
☒ ☐	Antibodies
☒ ☐	Eukaryotic cell lines
☒ ☐	Palaeontology and archaeology
☒ ☐	Animals and other organisms
☒ ☐	Clinical data
☒ ☐	Dual use research of concern

Methods

n/a	Involved in the study
☒ ☐	ChIP-seq
☐ ☒	Flow cytometry
☒ ☐	MRI-based neuroimaging

Flow Cytometry

Plots

Confirm that:

☒ The axis labels state the marker and fluorochrome used (e.g. CD4-FITC).

☒ The axis scales are clearly visible. Include numbers along axes only for bottom left plot of group (a 'group' is an analysis of identical markers).

☒ All plots are contour plots with outliers or pseudocolor plots.

☒ A numerical value for number of cells or percentage (with statistics) is provided.

Methodology

Sample preparation	Samples were collected from experimental cultures, where the desired number of cells was centrifuged and resuspended in buffer to a density of ~10^6 cells/mL for flow cytometry.
Instrument	SORP BD LSRII (IMED) Analytic Flow Cytometer
Software	Data were collected on the BF FACSDiva software, exported as FCS files, and analyzed on FlowJo 10.8.2.
Cell population abundance	Samples were solely analyzed via flow cytometry for population counting and not collected for further experiments. Population frequencies were assessed based on detection of fluorescent proteins present in populations of interest.
Gating strategy	Initial FSC-A/FSC-H gates were drawn to remove debris and minimize the frequency of aggregates observed in microbial samples. Subsequent gating cutoffs for GFP or mCherry fluorescence was determined via signals from negative, GFP only, and mCherry only controls that were prepared and analyzed on the day of each experiment.

☒ Tick this box to confirm that a figure exemplifying the gating strategy is provided in the Supplementary Information.